Numerical Modelling of Reinforced Concrete Walls Encased in Polyvinyl Chloride Stay-in-place Formwork

by

Adnan Azam

A thesis

presented to the University of Waterloo

in fulfillment of the

thesis requirement for the degree of

Master of Applied Science

in

Civil Engineering

Waterloo, Ontario, Canada, 2015

AUTHOR'S DECLARATION

I hereby declare that I am the sole author of this thesis. This is a true copy of the thesis, including any required final revisions, as accepted by my examiners.

I understand that my thesis may be made electronically available to the public.

Abstract

In structurally participating formworks, a new forming technique for reinforced concrete, referred to as stay-in-place formwork has recently emerged as a viable technique. This permanent new formwork system simplifies the construction process and reduces construction time. Two materials that are well-suited for this technique are fiber reinforced polymer and polyvinyl chloride.

This research presents a non-linear and three-dimensional finite element model for reinforced concrete walls with and without polyvinyl chloride stay-in-place formwork. There is a variety of commercial programs for three-dimensional finite element modelling, but they lack the ability to model a complex composite material such as reinforced concrete encased in a polyvinyl chloride stay-in-place forming system. For its high performance and extensive range of material modelling capabilities, the ABAQUS finite element package was used in the current study. Concrete was modelled using a concrete damage plasticity model, and steel bars were modelled using an elastic and perfectly plastic material. Perfect bond was assumed between concrete and steel. The polyvinyl chloride stay-in-place formwork was modelled using an elasto-plastic material. As with the concrete and steel, perfect bond was assumed between the polyvinyl chloride panels and the concrete.

Finite element results were validated using experimental results reported by Scott (2014). It was observed from the comparison that the proposed non-linear fine element model is capable of predicting the load capacity for the reinforced concrete walls with and without the polyvinyl chloride stay-in-place formwork. Predicted yield loads were in good agreement with the experimental data, with an average error of 6% for control walls, 7% for the polyvinyl chloride encased reinforced concrete walls with flat panels, and 3% for the walls encased with hollow panels. In addition, finite element ultimate (peak) loads showed good correlation with the experimental data. The average error for the control, flat panel and hollow panel encased walls were 3%, 3% and 13%, respectively.

A parametric study was conducted to investigate the effect of concrete compressive strength, thickness of polyvinyl chloride stay-in-place formwork, and the strength of polyvinyl chloride used in

stay-in-place formworks. It was observed that the concrete compressive strength has a significant effect on the flexural strength of polyvinyl chloride encased reinforced concrete walls. As expected, the thickness and strength of the polyvinyl chloride used have a proportional effect on the behaviour of the encased reinforced concrete walls.

Acknowledgements

After thanking God for giving me the strength and ability to complete this work, I would like to express my sincere thanks to my mother and my family who have instilled in me the drive and encouragement to complete this work.

I express my deepest gratitude to my supervisor, Dr. Adil Al-Mayah, for his support, encouragement, guidance and valuable advice during my program of study.

I acknowledge and thank the Department of Civil & Environmental Engineering at the University of Waterloo and my colleagues in the Civil Engineering Research group for their support.

Special thanks to Usman Ali for his assistance with ABAQUS.

Finally, I would like to acknowledge the financial support I received during my studies from NSERC and the University of Waterloo.

Dedication

To Dr. K. A. Soudki

Table of Contents

List of Figures

List of Tables

Chapter 1: Introduction

Reinforced concrete (RC) has become one of the most important and widely used building materials in many types of engineering construction. The strength, efficiency, economy and stiffness of RC make it an attractive material for a wide range of structure applications. Concrete can be poured into a system of formwork to produce structural elements such as walls, columns and beams. Reinforcement bars are placed within the formwork and concrete before casting.

Stay-in-place (SIP) formwork is a new permanent system, which simplifies the construction process and is already being used in construction projects throughout the world. This type of formwork system can be made of a variety of materials such as polyvinyl chloride (PVC), fiber reinforced polymers (FRP), galvanized steel, precast concrete and timber. While the traditional or engineered formwork system is removed when hardened concrete has achieved a sufficient strength, the SIP formwork becomes part of the finished structure, which provides benefits such as eliminating or reducing the need for stripping and false work (McClelland, 2007). This is particularly tempting for the construction of walls and tanks where the wall geometry remains consistent. It protects the concrete from environmental effects such as corrosion and freeze-thaw cycle damage as the PVC prevents water penetration. These benefits allow for reduced maintenance costs and enhanced structural capacity and ductility. Figure 1.1 shows an example of the PVC SIP formwork.

Figure 1.1: Example of Tank Construction using SIP Formwork (Scott, 2014)

An efficient way to determine the load carrying capacity and structural behaviour of RC walls encased in PVC SIP formwork is to perform full scale tests in a laboratory. However, experimental testing is expensive and time consuming and, as such, the finite element (FE) method has become a powerful computational tool that allows complex analysis of the nonlinear response of RC structures to be carried out in a routine fashion. This method can assist in studying the effect of different design parameters and their interaction on the response of RC structures. There is a variety of commercial programs for 3-D modelling, but they have limited options and may lack the ability to model a complex composite material such as RC encased in PVC SIP forming system. The nonlinear FE software ABAQUS is used for this purpose in the current study. It is known for its high performance and extensive range of material modelling capabilities in solving challenging simulation problems.

A 3-D FE model (FEM) was developed in this study using the concrete damage plasticity (CDP) model for static loading. The main purpose of this study is to improve the ability of FE analysis to predict

the behaviour of RC encased in PVC SIP forming system and to investigate the effect of different design parameters on the performance of the PVC encased RC walls.

The results of the FEM were compared against experimental results reported by Scott (2014). The development of a reliable analytical model will reduce the number of required test specimens for future development of PVC SIP systems.

The development of the analytical model for the response of RC walls encased in PVC SIP forming work is a challenge due to the following factors:

- There are no studies that have investigated the behaviour of RC beams encased in PVC using FEM.
- RC is a composite material made up of concrete and steel; both are very different in mechanical and physical behaviour. Adding PVC SIP with its nonlinear stress-strain behaviour makes modelling a uniquely challenging simulation problem.
- Modelling the interaction between concrete, steel, and PVC is a complex case because of the nonlinear behaviour of concrete even under a low level of loading.

1.1 Research Objectives

The specific objectives of this thesis are:

1- Develop a FEM to predict the behaviour of RC walls encased in PVC SIP formwork.

2- Validate the FEM outcomes using experimental results reported by Scott (2014).

3- Conduct a parametric study to investigate the effect of concrete compressive strength, thickness of PVC SIP formwork and strength of PVC used in SIP formwork.

1.2 Organization of Thesis

This thesis is organized into six chapters as follows:

- Chapter 1: Introduction – This chapter describes the research motivation, research objectives and scope, and thesis outline.
- Chapter 2: Background and Literature Review – This chapter provides a brief summary of previous research work on permanent formwork and encased PVC walls. Discussion on the FEM software package ABAQUS and analytical modelling of PVC is also presented.
- Chapter 3: Modelling Approach and Material Models – This chapter discusses the modelling approach used to model concrete, steel, and PVC elements. In addition, various available material models used to define the behaviour of concrete, steel, and PVC materials are discussed.
- Chapter 4: Development of Finite Element Model – This chapter presents the development and validity of FEM for predicting the yield and ultimate loads for reinforced concrete walls with and without PVC SIP formwork.
- Chapter 5: Discussion of Results – In this chapter, the comparison of FEM and experimental results are presented. The yield and ultimate loads, and load-deflection performance are presented. Strain response to loading is also discussed in this chapter.
- Chapter 6: Parametric Study – This chapter presents the effect of different parameters on the performance of PVC encased RC walls.
- Chapter 7: Conclusion and Recommendations – this chapter presents the summary, the main conclusion from the study and recommended areas for future work.

Chapter 2: Background and Literature Review

Formwork is the term given to either temporary or permanent molds into which concrete or similar materials are cast to form a particular shape. It should be capable of carrying all imposed dead and live loads apart from its own weight. It has been in use since the beginning of concrete construction. Formwork can be made out of a large variety of materials. Timber is the most common material used for traditional formwork. The disadvantage with timber formwork is that it will warp, swell and shrink. Moreover, due to depleting forest reserves and the increasing cost of timber, the use of alternative materials such as steel has become prominent. More recently, materials such as plastic and fiberglass are also being used for pre-fabricated formwork. The type of material to be used depends on the nature of the construction as well as the availability and cost of the material.

Generally, formwork comes in three main types: traditional timber formwork, engineering formwork system, and SIP formwork. The traditional timber formwork is built on site from timber or plywood. The engineering formwork system is built out of prefabricated modules using metal (usually steel or aluminum). The SIP formwork system, also assembled on site, uses prefabricated FRP.

In this chapter, a summary of the literature on SIP formwork is presented. This chapter also introduces SIP formwork, summarizes the experimental studies conducted using FRP and PVC SIP formwork, special attention being given to PVC SIP formwork. In addition, it provides a brief summary of the analytical studies on PVC SIP formwork and an introduction to FE analysis using ABAQUS. Finally, the research needs in this area are highlighted.

2.1 Stay-in-place Formwork

In literature, two types of permanent formworks have been defined: structurally non-participating and structurally participating. Structurally non-participating formwork does not participate in carrying construction loads, thereby reducing the time and cost required in forming. Structurally participating formwork, on the other hand, is designed to resist both construction and in-service loads. Permanent

formworks provide benefits such as removing and reducing the need for stripping, falsework and labor (McClelland, 2007). In structurally participating formworks, different forming techniques for RC called SIP forming system have recently emerged as a viable technique. This new permanent formwork system simplifies the construction process and reduces construction time. The most widely used SIP systems are made of FRP and PVC (Amr, 2014).

2.1.1 FRP SIP Formwork

FRP composite materials are made of fibers imbedded in a polymeric resin. They have high tensile strength, flexibility of application, light weight (compared to steel), and they are corrosion free. Moreover, FRP materials can be manufactured into various shapes such as bars, sheets, or laminates (ACI 440.R1-06, 2006). The FRP SIP formwork system can be efficiently used for concrete columns to reduce the amount of internal reinforcement and to increase the resistance of the concrete members against severe weather effects (Amr, 2014). A number of research projects have been conducted to investigate the performance of FRP SIP formwork system.

Rizkalla and Fam (2002) tested 20 concrete filled FRP tubes (CFFTs) with flexural and shear reinforcement under four-point bending to observe their flexural behaviour. Some of the specimens were cast with an inner longitudinal hole to create a wall thickness equal to the theoretical compression block of a solid concrete cylinder. Different parameters were investigated including the specimen cross sectional geometry, length, concrete strength and reinforcement ratio. The specimens with the internal hole showed an increase of 35% in strength to weight ratio while reducing the ultimate load capacity by 9%. In general, increase in the FRP tube cross-sectional area improved the stiffness and the moment capacity.

Mohamad and Masmoudi (2012) tested seven cylindrical concrete beams encased in FRP SIP structural formwork in four-point bending. The specimens were 2000 mm in length and 213 mm in diameter. All beams were reinforced either with six glass fiber reinforced polymers (GFRP) bars 16 mm in diameter or six steel bars 15 mm in diameter. They investigated the test variables: compressive strength

(30 MPa or 45 MPa), internal reinforcement (FRP or steel), fiber orientation, and FRP tube thickness (2.9 mm or 6.4 mm). Fiber orientation was 60° and 90° to the longitudinal direction. All concrete filled GFRP tubes (CFFT) specimens failed in shear at a higher deflection with increased stiffness. The combination of steel bar and GFRP tube improved the ultimate load of element from 130% to 200% and allowed higher ductility (86%). It was concluded that varying the FRP tube thickness and concrete strength did not significantly change the flexural performance of the specimens.

Dieter et al. (2006) investigated the performance and the failure mechanisms of an FRP SIP bridge deck system by separately testing FRP reinforced beams and slabs. The beam specimens were 200 mm deep, 914 mm wide and 2650 mm long, while the slab specimens were 2745 mm square with a 200 mm thickness. The specimens were composed of a top grid (mesh) of FRP bars to resist negative bending and FRP deck planks to resist positive bending. The FRP planks were actually flat panels stiffened with corrugated box sections. Ultimate strength results were significantly lower than predicted and the deck slab failed in punching shear. It was concluded that this reduction was due to the corrugation of the FRP plank which reduced the effective shear depth from 200 mm to 127 mm. Further tests revealed that the FRP plank was not acting as a fully composite section with the concrete and that the FRP formed concrete did not achieve a full composite action.

Nelson and Fam (2014) investigated the performance of FRP SIP structural forms and concluded that the structural response of the FRP SIP formwork system in terms of flexural stiffness and strength is similar to conventional RC bridge decks. However, FRP SIP systems differed from steel in several aspects, with the most significant and notable being their stress-strain behaviour. The steel failed in a ductile manner. On the other hand, FRP systems remained linear elastic until they suddenly failed at a decreased strain compared to the rupture strain of steel rebar. This reduction in ductility was reflected in many FRP formed elements where load capacity exceeded or met RC elements.

Gai et al. (2013) tried to improve the ductility of FRP SIP formwork systems by developing a FRP SIP formwork that confined concrete using FRPs in order to increase the ductility of the concrete.

Six slab specimens consisting of two 3000mm long GFRP box sections (100 mm height x 100 mm width x 8 mm thick) adhesively bonded to a 3000mm long, 300 mm wide molded GFRP grating, were tested in five-point bending. The concrete filled GFRP grating carried compression forces, while pultrude hollow box sections resisted the tensile forces. The sand-coated GFRP dowels (10 mm diameter) were also provided to connect both components. The concrete prevented a brittle failure of the composite sections and increased the ductility of the system. Even with these improvements, the modified formwork required an increased amount of FRP to establish ductility, which was a costly solution. The use of PVC SIP formwork could increase ductility at a much lower cost.

2.1.2 PVC SIP Formwork

PVC material is different from FRP in several ways. It has a lower strength than FRP, and offers significant benefits such as a lower cost and a higher rupture strain (Scott, 2014).

PVC SIP formwork consists of a system of panels and connectors. The panels form the concrete wall faces, while the connectors fasten the faces of the wall together. They interconnect on the construction site into a hollow wall shell structure which is then filled with concrete to form a complete wall (Figure 2.1). A series of openings in the interconnecting elements allow for easy installation of reinforcing steel and the lateral flow of concrete (Octaform 2004).The elements totally confine the RC wall structure resulting in an increase in the strength and durability of the structure (Octaform, 2004). The PVC SIP formwork system offers the advantage of a simplified construction process, especially in the process of building with consistent and continuous geometries. This system can be used for retaining walls, foundation walls, swimming pools, and water and waste treatment tanks. The SIP formwork system provides the feasibility to be assembled to create either straight or round walls. It provides additional tension reinforcement thereby increasing the capacity of the wall.

a - Connector

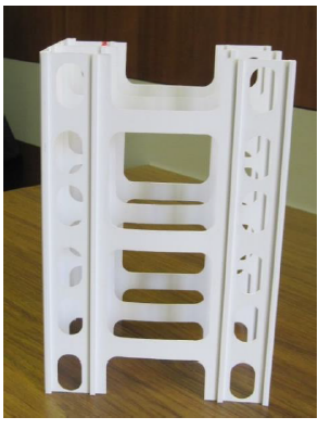

b – Side view of the wall cell

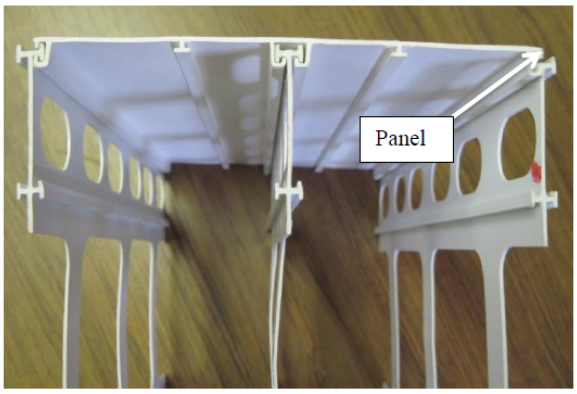

c – Top view of the wall cell

Figure 2.1: Elements used in PVC SIP Formwork (Scott, 2014)

Chahrour et al. (2005) experimentally investigated the flexural behaviour of concrete walls encased in a PVC SIP forming system (Royal Building System) with and without steel reinforcement. 15specimens of 2000 mm long and 233 mm wide were tested in four-point bending. The reinforcement ratio (un-reinforced, 1-10M rebar) and the thickness of the concrete wall (100, 150, and 200 mm) were investigated. Four un-reinforced PVC-encased specimens developed 'saw-tooth' load-deflection curves (Figure 2.2). At every concrete cracking point, there was either a sudden load drop and increase or a rebound as the PVC formwork panels resisted the tensile stresses. Several load drops or rebounds were observed at the cracking stage and continued until the deflection increased or the load level started to

drop. Rupture of PVC on the tension side was the cause of failure, as shown in Figure 2.3. The addition of reinforcement reduced the severity of the 'saw-tooth' jumps.

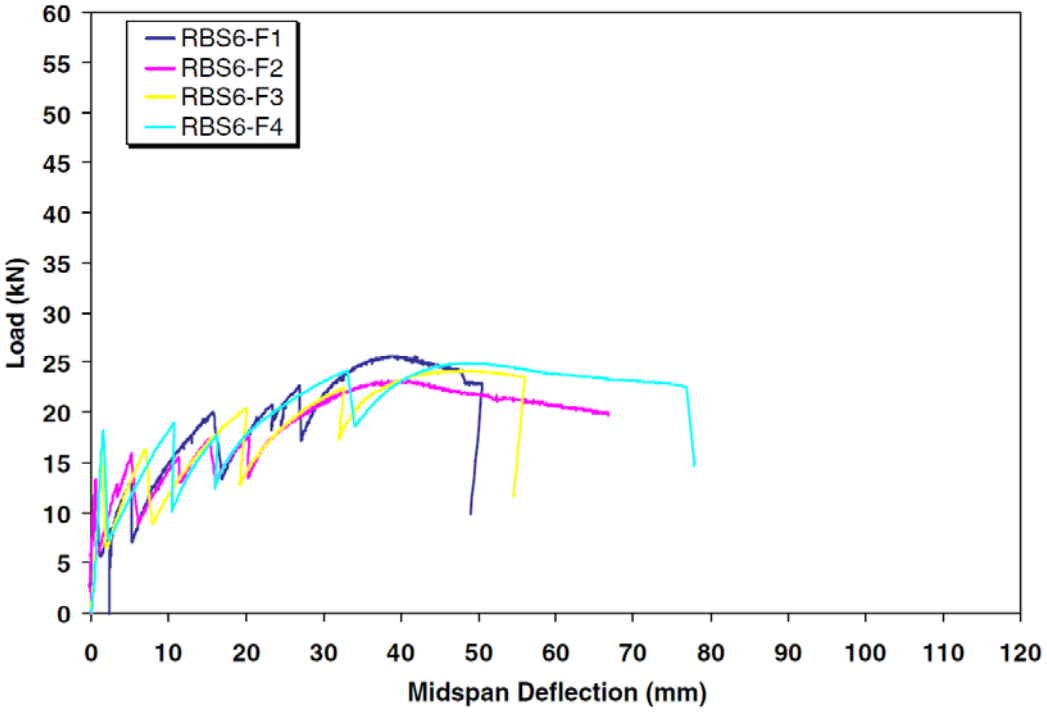

Figure 2.2: Load Deflection of Plain Concrete Encased in PVC SIP Formwork (Chahrour et al. 2005)

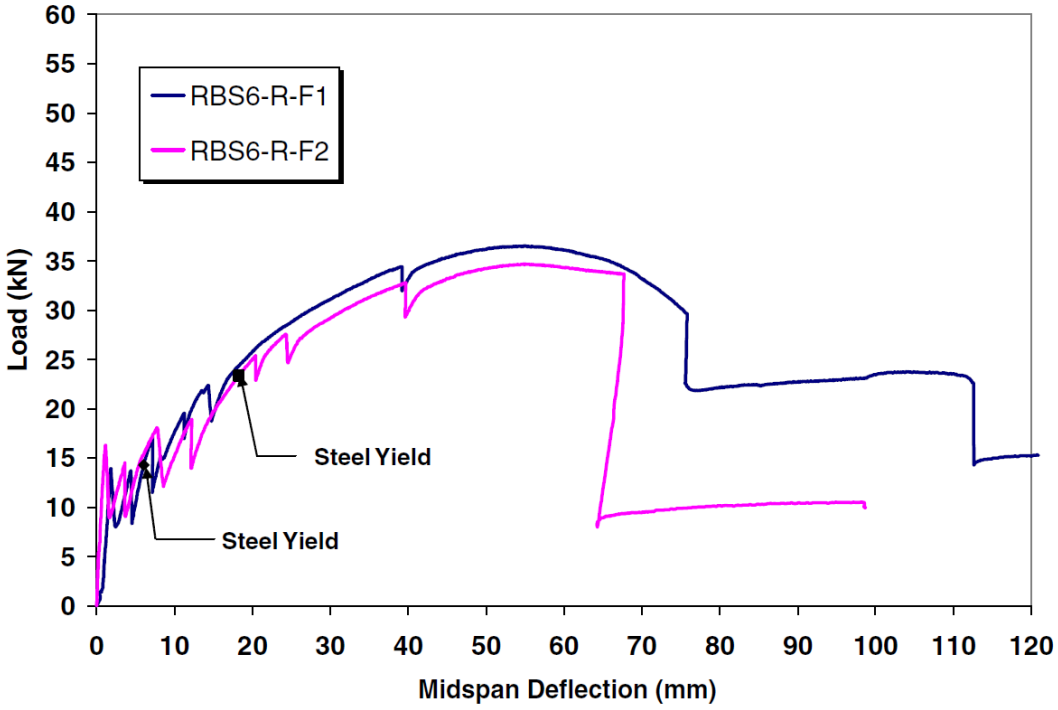

Figure 2.3: Load Deflection of PVC Encased Concrete (Chahrour et al. 2005)

As the core thickness increased, the ultimate load and ductility increased. In general, it was concluded that the PVC SIP forming system did not have sufficient strength to completely replace steel reinforcement in the concrete. Other materials such as steel or FRP would be required as an internal reinforcement.

Rteil et al. (2008) tested 20 concrete specimens encased in PVC formwork (Octaform System) under four-point bending. Specimens were 305 mm wide and 2500 mm long, test variables had a concrete core thickness of 150 mm or 200 mm, arrangement of the PVC connectors was middle or braced, and internal reinforcement was unreinforced or 2-10M bars. The concrete walls encased in PVC formwork system with no reinforcement showed an increase in the ultimate load capacity and ductility over concrete walls without PVC encasement. The increase was more distinct as the wall thickness decreased. The results showed that the PVC formwork system did not change the failure mode, nor did the connector's configurations affect the PVC SIP formwork performance. However, the PVC formwork enhanced the

ultimate load capacity by 36% for 150 mm thick walls and 18% for 200 mm thick walls. In addition, the PVC formwork system increased the deflection of the specimens by 24% and 55% for 150 mm and 200 mm thick walls, respectively.

Kuder et al. (2009) explored the effect of connector configuration on the mechanical performance of concrete walls. They cast four PVC encased concrete walls reinforced with 10M steel rebars using the Octaform system. Each specimen was 610 mm long, 152.4 mm wide, and 152.4 mm in thickness. The PVC connection configurations were different for each specimen, as shown in Figure 2.4.

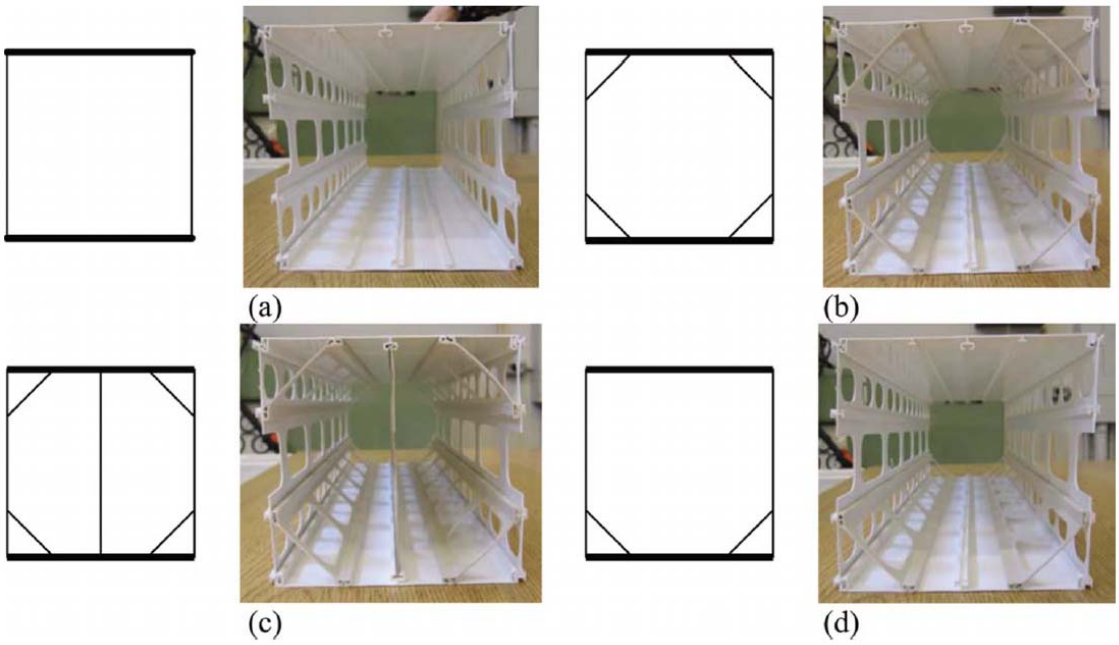

Figure 2.4: PVC Connectors' Arrangement (Kuder et al. 2009)

The PVC encased walls were tested under three-point bending with a shear span of 254 mm. It was concluded that there was improvement in the flexural capacity and toughness in the PVC encased specimens over the non-encased control specimens. The improvement varied from 39% to 66% and 41% to 60%, respectively. The cross-section shown in Figure 2.4- c with the highest quantity of PVC polymer showed the highest increase in the ultimate load.

Wahab and Soudki (2013) investigated the flexural behaviour of concrete walls encased in PVC SIP forming system on a large number of specimens. They tested 24 specimens under four-point bending with a shear span of 1150 mm. The specimens were 3050 mm long, 457 mm wide, 200 or 250 mm thick and were cast in two batches using a concrete strength of 43 MPa and 54 MPa, respectively. Test variables were steel rebars with a reinforcement ratio of 3-10M, 3-15M or 3-20M, middle or braced PVC connectors, and a specimen thickness of 200 mm or 250 mm. The PVC encased specimens showed an increase in cracking, yielding, and ultimate loads over the concrete specimens without PVC encasement. Wahab and Soudki reported that the contribution of the PVC formwork system to the ultimate load increased as the reinforcement ratio decreased. They also reported a 17.4% to 37.7% increase in the ultimate load and a 2.5% to 200% increase in ductility due to the PVC SIP formwork. From the test data, it was concluded that the PVC connectors did not have any effect on the flexural strength of the PVC encased concrete specimens, suggesting that they could be ignored.

Scott (2014) further explored the flexural behaviour of SIP PVC encased RC. Using standard analysis techniques, he performed experimental testing to prove that system capacity is significantly larger than the strength calculated and to determine how the strength and deflection of RC changes with the addition of the PVC SIP forming system. For this testing, 18 specimens were cast in total: six specimens were cast without PVC encasement to act as control walls, and the remaining 12 specimens were cast using the PVC forming system. The walls were tested in four-point bending using a servo-hydraulic actuator controlled by an MTS-Digital GT controller. Two types of PVC formwork panels were used: flat and hollow panels (Figure 2.5).

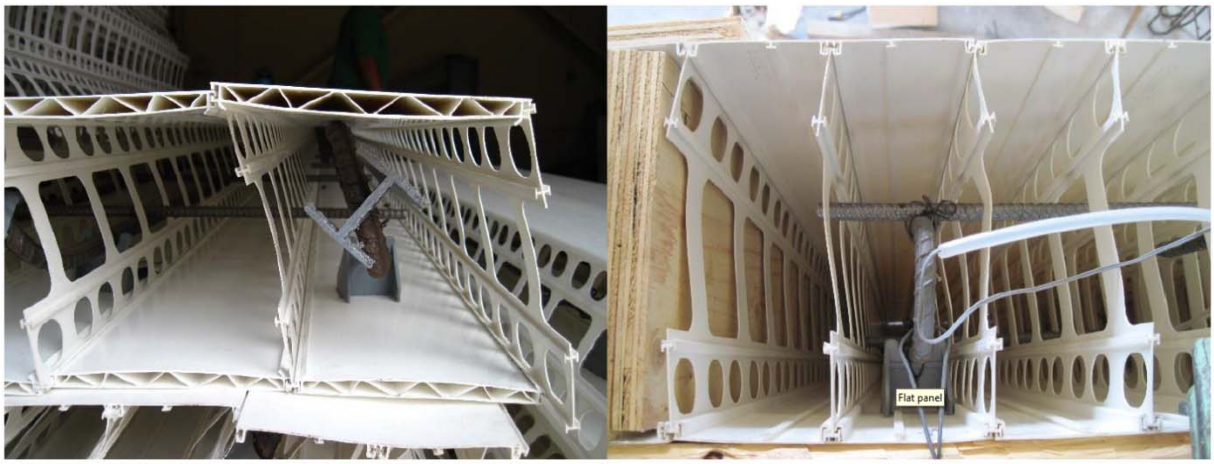

Figure 2.5: Examples of Assembled Hollow Panel and Flat Panel Walls (Scott, 2014)

All six control specimens exhibited the same failure mechanism. According to the failure modes, the reinforced steel yielded at mid span followed by concrete crushing in the constant moment region. Most of the crushing failure occurred at mid span and the crushing locations were close to the right loading point. Once the steel yielded, the cracks in the constant moment region (at mid span) widened significantly as the curvature of the wall increased. The specimens showed the same load versus deflection behaviour, which can be described in three distinct phases: un-cracked, cracked and post yield. The un-cracked phase exhibited a rapid rise in load with minimal deflection. In the cracked phase, the load increased linearly with deflection as the stiffness decreased compared to the un-cracked phase. At the post-yield phase, the deflection of the specimen increased rapidly with little increase in load. It was concluded that the cracking load was controlled by the specimen thickness; it increased with the increase of thickness. The yield load was a function of the quantity of tension steel reinforcement at a constant core thickness; the load increased with the increase in the rebar diameter. Furthermore, the increase of concrete core thickness increased the yield load.

All the PVC encased walls with flat panels cracked in a similar manner and experienced the same failure mode for a given tension steel reinforcement quantity. The flat panel specimens showed the significant improvement in applied load and ductility. The PVC encased walls with flat panels showed a

higher yield load than the control wall specimens. The ultimate deflection of the PVC encased walls was significantly higher than the ultimate deflection of the control wall specimens. Specimens reinforced with 15M rebars failed in the same manner, but did not experience PVC rupture. The flat panels increased the cracking load by an average of 70%, the yield load by 17% and the peak load by 33% over the control wall specimens. Encasement also increased, with the ultimate deflection varying between 32% and 106%, and the ductility index varying between 24% and 167%. The toughness of the PVC encased walls with flat panels increased significantly (ranging from 57% to 170%) over the control walls.

A new phenomenon was observed during testing of the PVC encased walls with hollow panels. The slip of panels resisted the tensile forces at the bottom of the walls. This occurred at a higher load level and at multiple times after steel yielding. In general, an average increase of 45% in the cracking load and 39% in the peak load over control walls were reported.

2.2 Analytical Modelling of PVC SIP Formwork

In almost all previous studies, the PVC SIP formwork was modelled through the development of an analytical model (Chahrour, 2005; Rteil, 2008; Kuder, 2009; Wahab and Soudki, 2013). The key aspect of using the analytical model was to predict the ultimate load capacity of the PVC formed concrete elements. Most of these studies were limited to a linear strain analysis except for a study conducted by Wahab and Soudki, 2013 where the non-linear stress-strain behaviour of the PVC formwork was investigated. They used Equation (1-1) to calculate the non-linear stress-strain behaviour of the PVC formwork provided by the manufacturers. The stress distribution and strain profile are presented in Figure 2.6. To describe the interaction between the concrete and the PVC, a composite action or perfect bond was assumed. The analytical model results showed good agreement with the test results, with an average error of 5%.

$$\sigma_{PVC} = -71518 * \varepsilon_{PVC}^2 + 3412.1 * \varepsilon_{PVC} \qquad Eq\ (1.1)$$

Where;

- ε_{PVC} is the strain in the PVC.
- σ_{PVC} is the corresponding stress at that strain level.

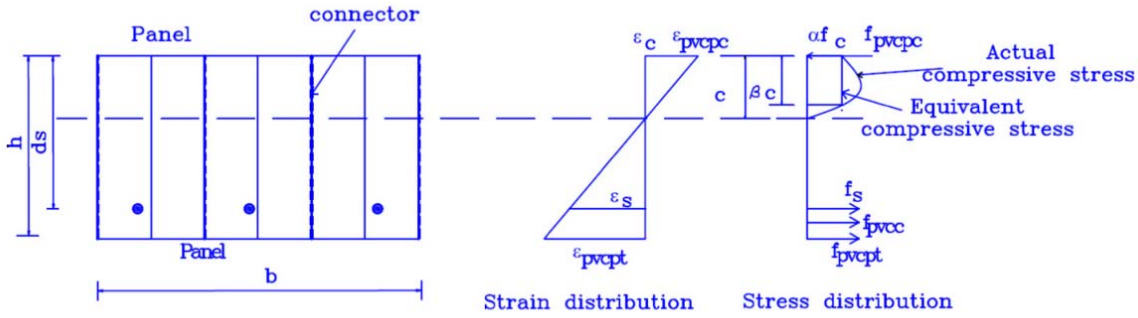

Figure 2.6: Stress-Strain Distribution of PVC SIP Formwork Cross-Section. (Wahab and Soudki, 2013)

2.3 Introduction to ABAQUS

The most reliable method to evaluate the behaviour of RC structures is through experimental investigation of actual structural members. Unfortunately, this is not always possible due to expense and time commitment. Instead, a FEM technique has been used in this research project. While different FEM software is available, ABAQUS was selected for this study.

ABAQUS is known for its high performance and extensive range of material modelling capabilities to solve different challenging simulations in FE analysis, more than any other software. The ABAQUS software package basically offers three core products: Standard and Explicit, Computational Fluid Dynamics (CFD), and Electromagnetic modules. Each of these packages offers additional optional modules that address specialized capabilities. The ABAQUS Standard analysis is powered with the widest range of contact and nonlinear material options and is used to solve traditional implicit FE analysis, such as static, dynamics, and thermal. The ABAQUS Standard analysis was used in this study.

The ABAQUS software package offers different models of inelastic behaviour to represent a wide range of potentially brittle materials, such as metals, soils, cost iron and concrete. There are two

main types of constitutive models available in ABAQUS for the inelastic behaviour of concrete: concrete damage plasticity (CDP) and smeared cracking (SC).

2.4 Research Needs

The literature review has revealed that there remain gaps in the state-of-knowledge on the PVC encased RC walls. To the best of the author's knowledge, there has not been a single study conducted to investigate the effect of PVC thickness and strength on the performance of PVC encased RC walls. In addition, no study in the literature has reported the effect of concrete strength used in formwork on behaviour of PVC encased RC walls. The current study intends to improve our understanding in this area.

Chapter 3: Modelling Approach of Material Models

In this chapter, the modelling approach for both RC walls and PVC encased RC walls is presented. Material models used for concrete, steel rebar and PVC are also presented.

3.1 Modelling Approach

3.1.1 Concrete

3.1.1.1 General

Concrete is a non-homogeneous material comprised of cement, aggregate and water. Aggregates and cement paste have a linear and brittle stress-strain relationship in compression. However, when mixed, the resulting mixture exhibits non-linear and somewhat ductile stress-strain relationship under compression. This is as a result of the redistribution of stresses within the complex matrix and a gradual development of micro cracking. The other reason for concrete non-linearity may be attributed to its porosity which causes non-uniform stress distribution when concrete is loaded. Hence, the composite nature of concrete provides a difficult challenge in modelling applications.

Although concrete is assumed to be isotropic, the interaction between the individual constituents causes concrete to behave differently under different loading, such as compression and tension. Typical concrete exhibits much greater compressive strength than tensile strength due to the bond between the aggregates and the cement paste. Depending on the type of tensile test, the tensile strength of the concrete is approximately in the range of 8% to 15% of the compressive strength.

In RC, the composite interaction between the concrete and the reinforced steel must also be considered. Although, the FEM is considered a reliable tool for the analysis of complex engineering problems, it does not fully capture the cause of micro cracks, thus there is always a difference between the experimental and numerically modelling results. ABAQUS software (SIMULIA 2011) provides the

capability to simulate the composite nature of RC using either one of three crack models: smeared cracking model (SC), concrete damage plasticity model (CDP), and brittle crack concrete model. It was decided that the best method to adopt for this study was CDP because of its potential to represent a complete inelastic behaviour under compression and tension.

3.1.1.2 Concrete Damage Plasticity (CDP) Model

The CDP model was proposed by Lubliner et al. (1989) and modified later by Lee and Fenves (1998). CDP is capable of modelling all structural types of reinforced and unreinforced concrete subjected to monotonic, cyclic or dynamic loads.

This model assumes that the two main failure mechanisms in concrete are the compressive crushing and tensile cracking. Therefore, it requires compressive and tensile input parameters to accurately model the material behaviour. These parameters include the elastic modulus, the Poisson's ratio, and the stress-strain behaviour of concrete in compression and tension. Due to the small thickness and low strength of PVC material, the confinement effect was not considered in the material model of concrete. Similar assumption has been made in previous analytical studies on SIP formwork system (Rteil et al 2008). In addition, the model requires plastic damage parameters. These plastic damage parameters include the dilation angle (ψ), the flow potential eccentricity, the ratio of initial equi-biaxial compressive yield stress (f_{b0}) to initial uniaxial compressive yield stress (f_{c0}), the ratio of second stress invariant on the tensile meridian to that of the compressive meridian (K), and the viscosity parameter that defines visco-plastic regulation (ABAQUS Documentation, 2011).

The CDP model needs a complete stress-strain curve of concrete under compression to define the compressive behaviour. The stress-strain curve can be defined beyond the ultimate stress into the strain softening region. Two parameters are required to be defined in the tabular format, namely: the compressive stress (σ_c) (i.e., yield stress in the data entry column), and the inelastic strain $\tilde{\varepsilon}_c^{in}$.

The compressive stress (σ_c) vs. strain (ε_c) data can be obtained through material testing or proper numerical technique. A numerical technique (presented in Section 3.2.1) was used in the present study as

an alternative to the material tests. The inelastic strain ($\tilde{\varepsilon}_c^{in}$) is defined by using Equation 3.1 in terms of total compressive strain (ε_c), and the elastic strain (ε_{oc}^{el}) corresponds to the undamaged material.

$$\tilde{\varepsilon}_{oc}^{in} = \varepsilon_c - \varepsilon_{oc}^{el} \qquad Eq.(3.1)$$

Where elastic strain (ε_{oc}^{el}) was calculated from Equation 3.2 as below.

$$\varepsilon_{oc}^{el} = \frac{\sigma_c}{E_0} \qquad Eq.(3.2)$$

E_0 is the Young's modulus of concrete.

The concrete damage in compression (d_c), should be defined if unloading steps are involved during the simulation. In such situations, the plastic strain ($\tilde{\varepsilon}_c^{pl}$) values should be calculated using Equation 3.3.

$$\tilde{\varepsilon}_c^{pl} = \tilde{\varepsilon}_c^{in} - \frac{d_c}{(1-d_c)}\frac{\sigma_c}{E_0} \qquad Eq.(3.3)$$

The compressive inelastic strain $\tilde{\varepsilon}_{oc}^{in}$ is defined as the total strain minus the elastic strain, as illustrated in Figure 3.1.

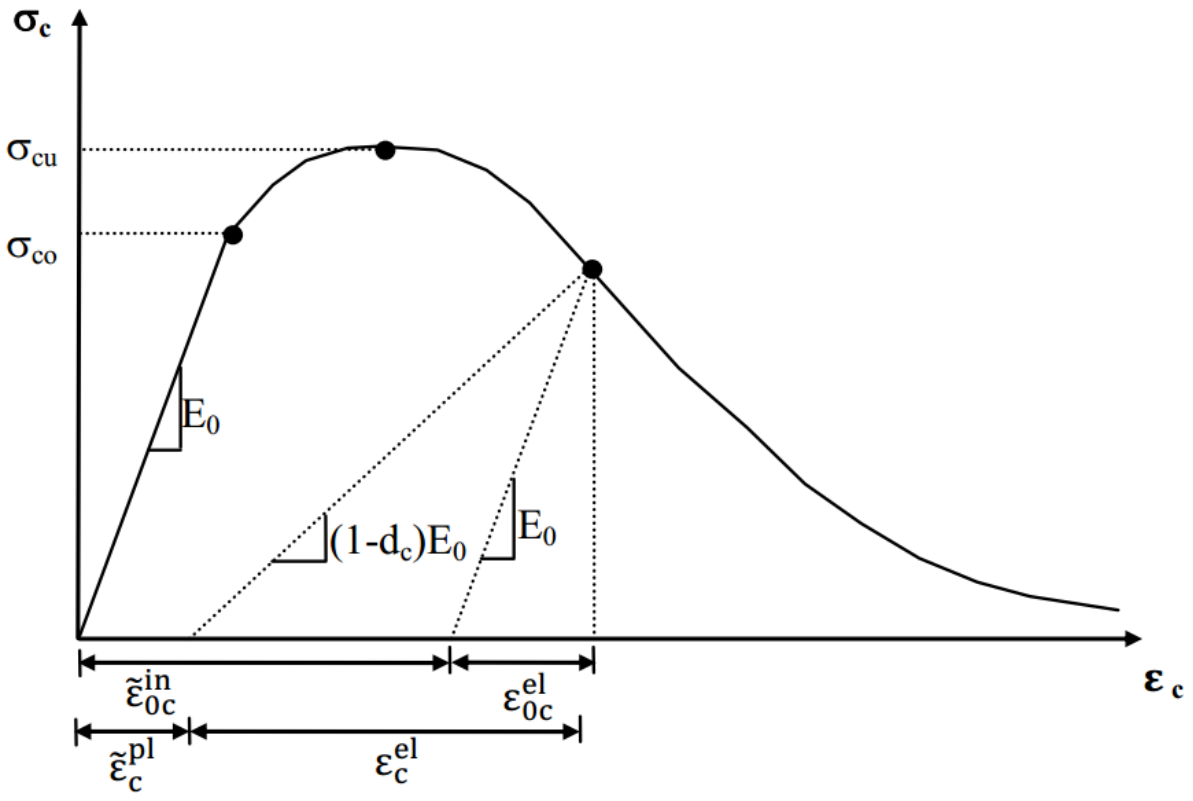

Figure 3.1: Compressive Stress-Strain Relationship (ABAQUS Manual, 2011)

The post cracking behaviour of RC structures is governed by the stress-strain relationship of concrete under tension. Concrete behaviour in tension was modelled using a linear elastic approach until cracking was initiated at the tensile strength level, after which crack initiation softening started. The post failure behaviour was modelled with tension softening, which allowed one to define the strain softening behaviour for cracked concrete. A typical stress-strain curve under tension (including non-linear region) is presented in Figure 3.2.

The cracking strain values ($\tilde{\varepsilon}_t^{ck}$) versus the tensile stress (σ_t) must be provided in a tabular format to define the complete stress-strain curve. The cracking strain can be calculated from Equation 3.4.

$$\tilde{\varepsilon}_t^{ck} = \varepsilon_t - \varepsilon_{ot}^{el} \qquad Eq.\ (3.4)$$

Where, ε_t is the total strain, and ε_{ot}^{el} is the strain corresponding to the undamaged material and calculated using Equation 3.5.

$$\varepsilon_{ot}^{el} = {}^{\sigma_t}/_{E_0} \qquad Eq.\ (3.5)$$

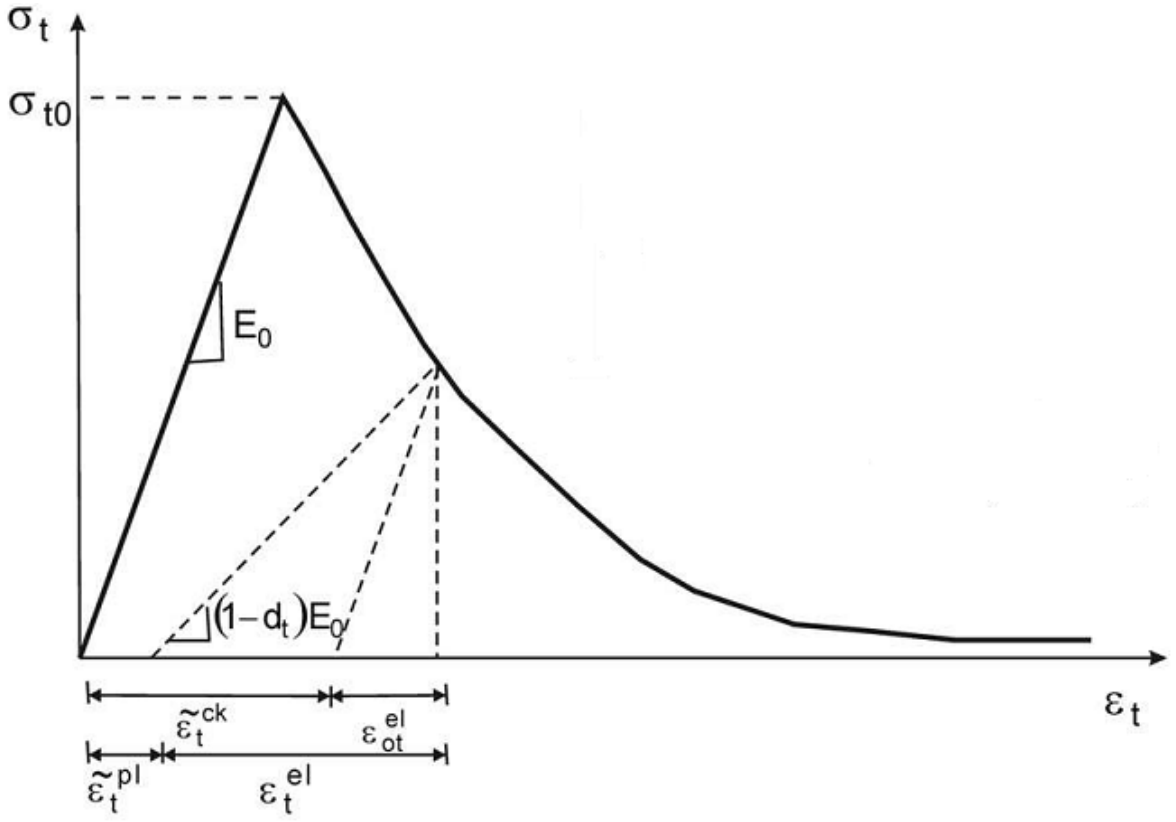

Figure 3.2: Tension Stiffening Model (ABAQUS Manual, 2011)

The concrete damage in compression (d_c), should be defined if unloading steps are involved during the simulation. In such situations, the plastic strain ($\tilde{\varepsilon}_t^{pl}$) values should be calculated using Equation 3.6.

$$\tilde{\varepsilon}_t^{pl} = \tilde{\varepsilon}_t^{ck} - \frac{d_t}{(1-d_t)}\frac{\sigma_t}{E_0} \qquad Eq.\ (3.6)$$

3.1.2 Steel Rebar

Currently, there are four methods available to model the reinforced bars in the FEM. In each method, the nodes of rebar are embedded and constrained with the nodes of the host concrete elements. The type of rebar element depends on the host element capabilities. Therefore, when concrete elements

are solid, rebar elements may be defined as beam, truss, shell, membrane, surface or solid elements (ABAQUS Documentation, 2011). The technique selected for this study was to model the steel rebar as three-dimensional elements. Details of the elements for steel rebar modelling are discussed in Chapter 4.

3.1.3 PVC SIP Formwork

3-D shell elements were selected to model the PVC SIP forming system. There were many issues with modelling it as a 3-Dsolid member, especially related to meshing and its interaction with concrete. Details of the elements for PVC SIP forming system are discussed in Chapter 4.

3.2 Material Models

For a realistic FEM, it is essential to include the material behaviour as accurately as possible as the proper selection of constitutive models plays an important role. Material properties can play an important role when undertaking any kind of non-linear FE analysis. In this section, the various constitutive relationships used to get the necessary input data for each material involved are presented.

3.2.1 Concrete

Concrete under uniaxial compression behaves in a non-linear manner following a small linear portion. ABAQUS uses the elastic definition to determine the material response until the material reaches the defined cracking stress, after which the non-linear behaviour of the material governs. These material properties are defined using the "elastic" command within the ABAQUS software package. For this behaviour, the modulus of elasticity is defined for concrete (E_c), as well as the Poisson's ratio (υ). The Poisson's ratio of concrete ranges from 0.15 to 0.22; a representative value of 0.19 or 0.20 (ASCE Task Committee and Masonry Structure, 1982). In this study, the Poisson's ratio of concrete is assumed to be 0.20.

As stated previously, the CDP model was selected for this study. To properly define the CDP, many different commands need to be utilized. The first of these is the damage plasticity command which

defines the five plastic damage parameters as discussed earlier in Section 3.1.1.2. The values used for these parameters are presented in

Table 3-1.

Table 3-1: Parameters for Concrete Damage Plasticity Model

Parameter	Value
Dilation Angle ψ	30
Eccentricity	0.1
f_{b0}/f_{c0}	1.16
K	0.667
Viscosity Parameter	0.01

3.2.1.1 Compressive Stress-Strain Curve

To define uniaxial compressive stress-strain behaviour in the CDP model, the compressive behaviour command was used. As discussed in Section 3.1.1.2, the constitutive behaviour of concrete was determined using the concrete damage plasticity model in ABAQUS.

The numerical method proposed and experimentally validated by Collins and Mitchell (1987) was used to obtain the complete stress-strain relationships for all simulated case studies in this study. For compressive strength less than 41 MPa, concrete is assumed to follow a parabolic stress strain relationship. The concrete used for this study was tested in the laboratory and showed a cylinder strength after 28 days of 21.8±0.7 MPa (Scott, 2014). The stress-strain expression can be expressed using following equations:

$$f_c = f_c' \left(\frac{2\varepsilon}{\varepsilon_o} - \left(\frac{\varepsilon}{\varepsilon_o} \right)^2 \right) \qquad Eq. (3.7)$$

$$\varepsilon_o = \frac{2f_c'}{E_c} \qquad Eq. (3.8)$$

$$E_c = 4500\sqrt{f_c'} \qquad Eq.\ (3.9)$$

Where:

f_c: the concrete stress corresponding to a given concrete strain,

f_c': the concrete compressive strength,

ε: the concrete strain corresponding to a given concrete stress,

ε_o: the concrete strain corresponding to the concrete compressive strength, and

E_c: the Young's modulus of concrete.

The expression provides the basis for input data in ABAQUS to describe the compressive behaviour of concrete. Figure 3.3 shows the compressive stress vs. compressive strain relationship used for this study.

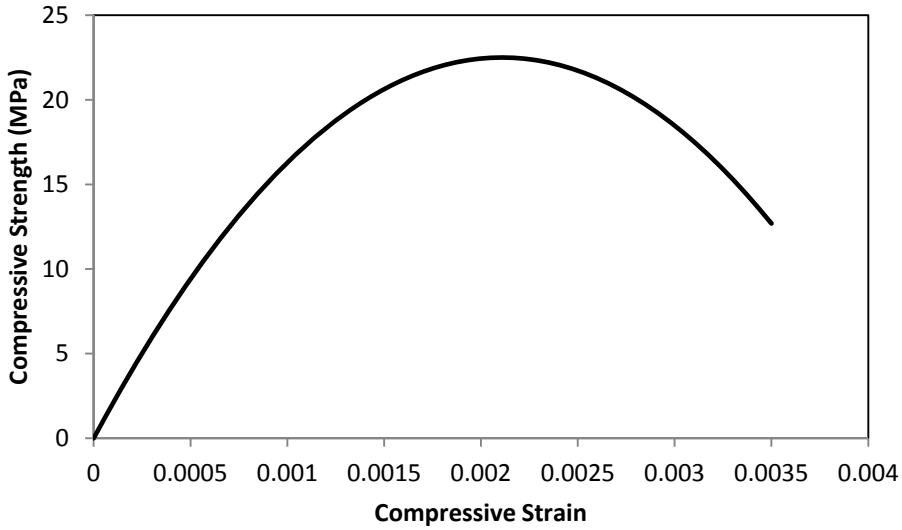

Figure 3.3: Compressive Behaviour of Concrete

3.2.1.2 Tensile Stress-Strain Curve

The tensile behaviour command was used to define the tensile stress-strain curve in the model. Under uniaxial tension, concrete experiences tensile cracking. The failure stress corresponds to the onset of micro-cracking in the concrete material; however, beyond the failure stress, the formation of micro-cracks is represented macroscopically with the softening stress-strain response. The Kmiecik and Kaminski (2011) model was used to drive the stress-strain curve (Figure 3.4) using the following equations:

$$\sigma_t = E_{co}\varepsilon_t \; for \;\; \varepsilon_t \leq \varepsilon_{cr} \qquad Eq.\,(3.10)$$

$$\sigma_t = f_t' \left(\frac{\varepsilon_{cr}}{\varepsilon_t}\right)^{0.4} for \;\; \varepsilon_t > \varepsilon_{cr} \qquad Eq.\,(3.11)$$

Where:

$$E_{co} = 5000\sqrt{f_c'} \qquad Eq.\,(3.12)$$

$$\varepsilon_{cr} = \frac{f_c'}{E_{co}} \qquad Eq.\,(3.13)$$

$$f_t' = 0.33\sqrt{f_c'} \qquad Eq.\,(3.14)$$

In Equation 3.8 and 3.9, E_{co} is the initial modulus of elasticity, ε_t is the concrete tensile strain, f_t' is the tensile strength of concrete (peak stress), and ε_{cr} is the concrete strain at peak stress (at cracking). Equation 3.9 was first proposed by Tamai (1988) and has since been used by many researchers including Belarbi and Hasu (1994), Hasu and Zhang (1996), and Wang and Hasu (2001). Kmiecik and Kaminski (2001) introduced a modified version for the post-peak response:

$$\sigma_t = f_t' \left(\frac{\varepsilon_{cr}}{\varepsilon_t}\right)^{n} for \;\; \varepsilon_t > \varepsilon_{cr} \qquad Eq.\,(3.15)$$

As the magnitude of tension stiffening significantly influences the response of a reinforced structure, Equation 3.13 allowed us to study various post-peak responses by introducing a variable n (as n increases the rate decay of tensile capacity increases) to control the rate of strength degradation.

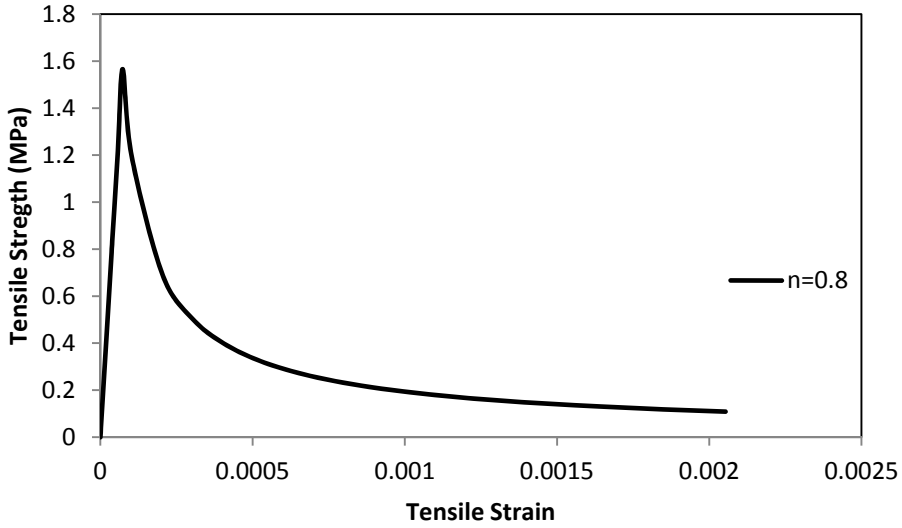

Figure 3.4: Tensile Behaviour of Concrete

3.2.2 Steel

Reinforced steel bars of 10M with a yield stress of 486 MPa were used in this study, as reported by the manufacturer. Standard elastic steel material property inputs were specified for the rebar, which included the following assumptions: the modulus of elasticity of the rebar (E_S) was assumed to be 200 GPa, and the Poisson ratio (υ) was assumed to be 0.3. The tension reinforcement was assumed to be elastic until yielding. After yielding, plastic behaviour was assumed with a 1% strain hardening (Bi-linear behaviour) (Scott, 2014). The equations for stress-strain expression are:

$$f_s = \varepsilon_s E_s \qquad Eq.\ (3.16)$$

$$f_s = f_y + 0.01E_s(\varepsilon_s - \varepsilon_y) \qquad Eq.\ (3.17)$$

Where, f_s is the steel stress corresponding to a given steel strain (ε_s) and f_y is the steel stress corresponding to the steel yield strain (ε_y). The elastic and plastic commands were used as input properties in the FE models. Figure 3.5 shows the stress-strain relationship of 10M steel bar.

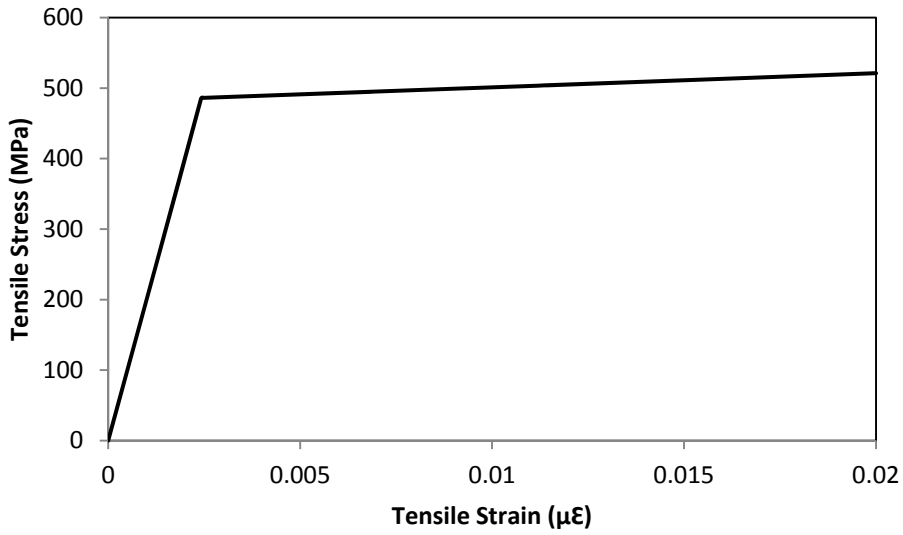

Figure 3.5: Tensile Behaviour of Steel Bar

3.2.3 PVC

The reported ultimate tensile strength and modulus of elasticity of the PVC based SIP forming system are 40.6 MPa and 2900 MPa, respectively, while the Poisson's ratio is 0.33 (Chahrour, et al. 2004 and Scott, 2014). These properties are defined by using the elastic command in the ABAQUS FE modelling package. The relationship shown in Figure 3.6 can be expressed according to the following equation:

$$f_{PVC} = -71518\varepsilon_{PVC}^2 + 3412.1\varepsilon_{PVC} \qquad Eq.\ (3.18)$$

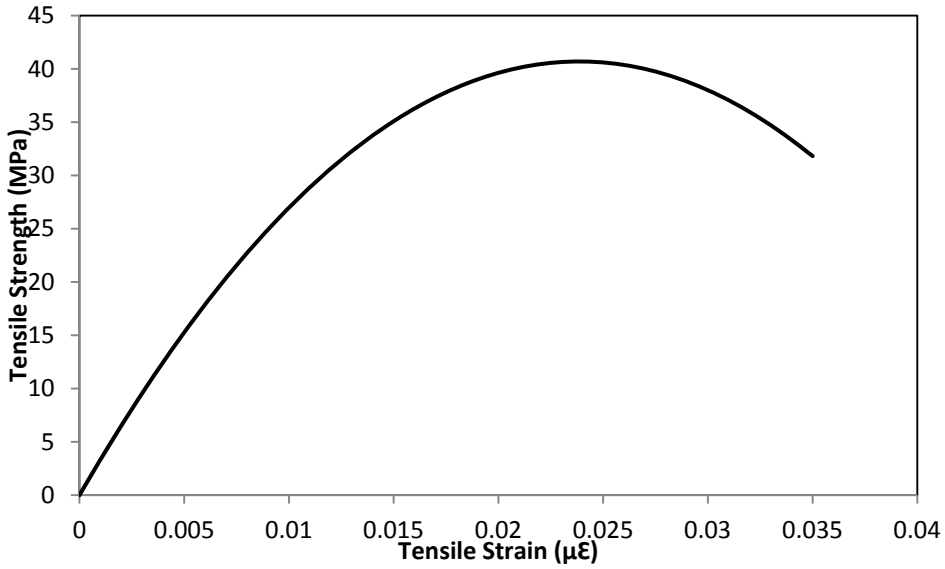

Figure 3.6: Tensile Behaviour of PVC

Chapter 4: Development of Finite Element Model

4.1 Introduction

This chapter describes the details the FEM developed to simulate the behaviour of RC walls with and without PVC encasement.

FE analysis has been used in this study due to its ability to model the complex behaviour of reinforced concrete such as cracking, tension stiffening, non-linear material properties, and reinforced concrete interface. The compressive and tensile stress-strain material models introduced in Chapter 3 were used in the analysis.

A total of 42 3-D non-linear FE analyses were performed using ABAQUS (2011). The FE model was validated by comparing the obtained load-midspan deflection behaviour, yield load, and peak load of walls with the experimental results conducted by Scott (2014).

4.2 Numerical Model Description

Complete ABAQUS environment (CAE) provides a complete interactive environment for creating ABAQUS models, submitting and monitoring analysis jobs, and viewing and manipulating simulation results. All parts making up the model were created in ABAQUS CAE (2011), which means they were not imported from other pre-processing software.

4.2.1 Beam Geometry

The experimental parameters used by Scott (2014) were applied in this work as inputs in order to validate the modelling technique. The tested walls reported were 2440 mm long and 610 mm wide. Different core thicknesses of specimens were investigated: 152 mm, 178 mm, or 203 mm (Figure 4.1). Each specimen was reinforced in the longitudinal direction with three steel rebars (3-10M) with clear cover of 38 mm on the tension side of the wall. In addition, specimens encased in various PVC SIP formworks were investigated, namely: flat panel formwork and hollow panel formwork (Figure 2.5).

Equivalent thickness of PVC formwork was used in modelling that was calculated based on the equivalent area.

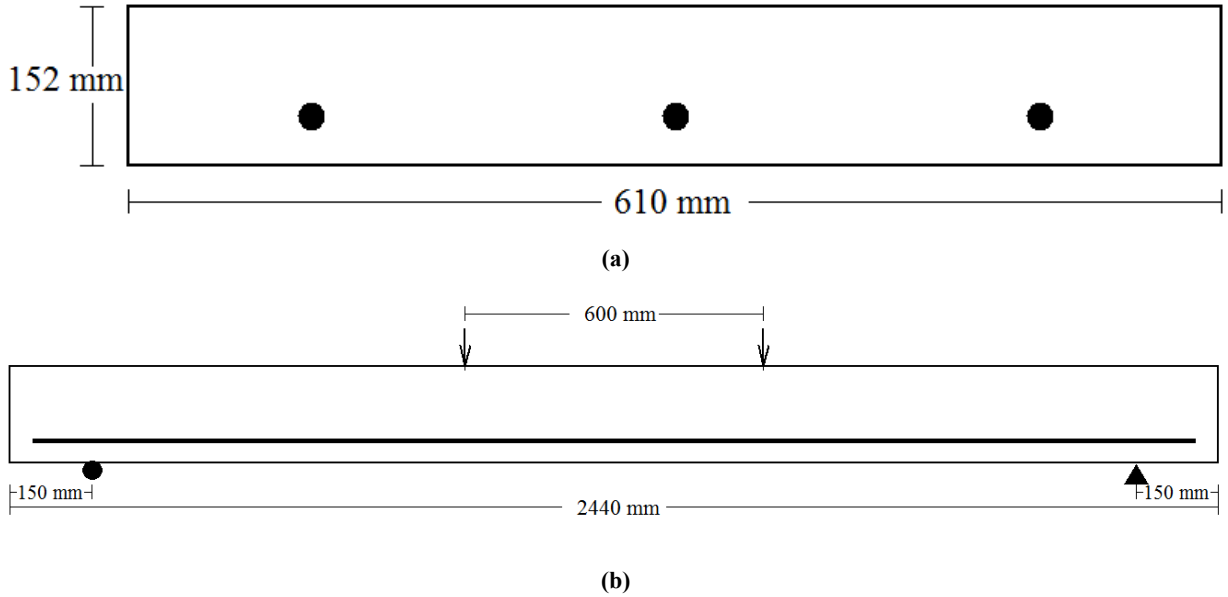

Figure 4.1: a) Cross-Section of RC Control Wall, and Tested Beam Details and Location of Point Loading for b) Control Wall Specimens.

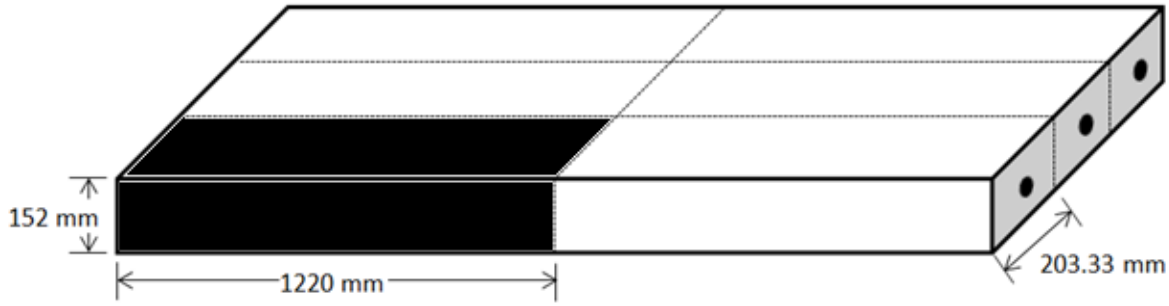

Figure 4.2: The Modelled 1/6th Wall Section

Based on the geometry, material properties, symmetric loading, and boundary conditions, a 1/6th FEM was built (Figure 4.2). The advantage of building 1/6th models for the tested wall specimens is the reduction in the total number of elements which resulted in significant savings of computational time (PKM, 2013; Obaidat, 2011; Wei, et al. 2014). The symmetrical boundary conditions were developed by

inserting vertical restraint (rollers) at each node located in the two planes of symmetry in the transverse and longitudinal directions. The beam and steel rebar geometries were created as 3-D deformable solid parts, while the PVC SIP forming system was created as a 3-D shell extrusion part (Figure 4.3).

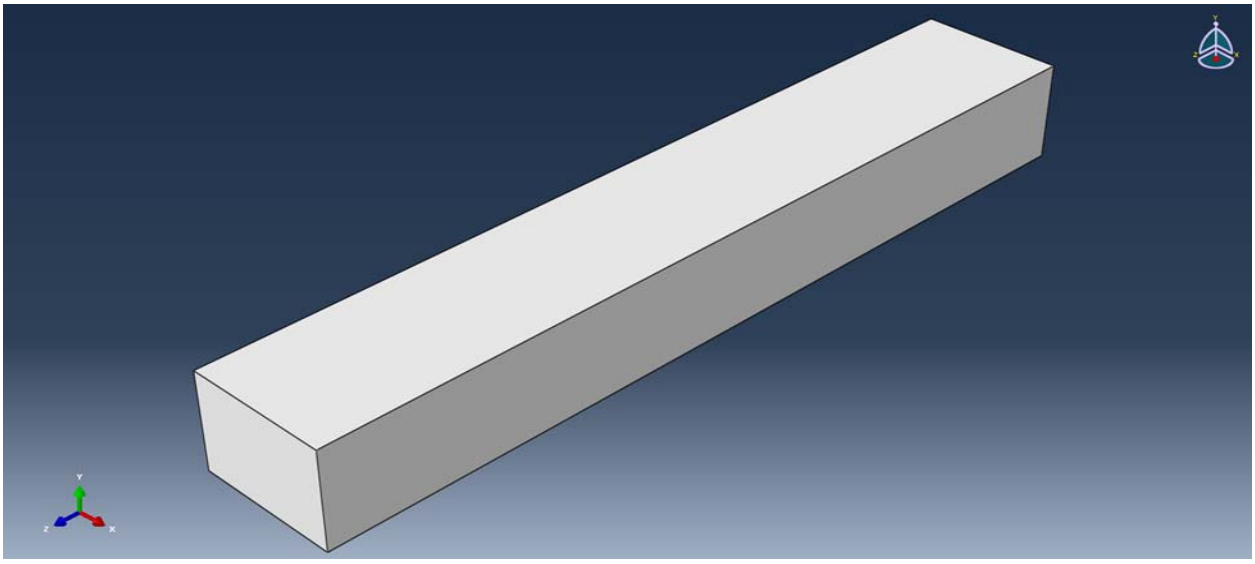

a) Concrete Beam

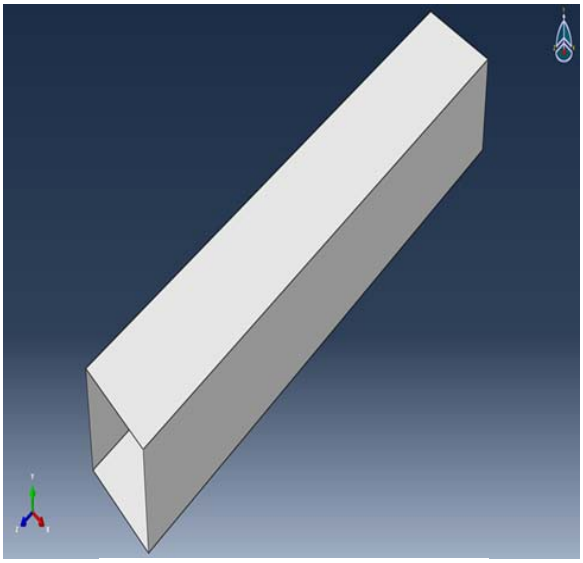

b) PVC SIP Formwork

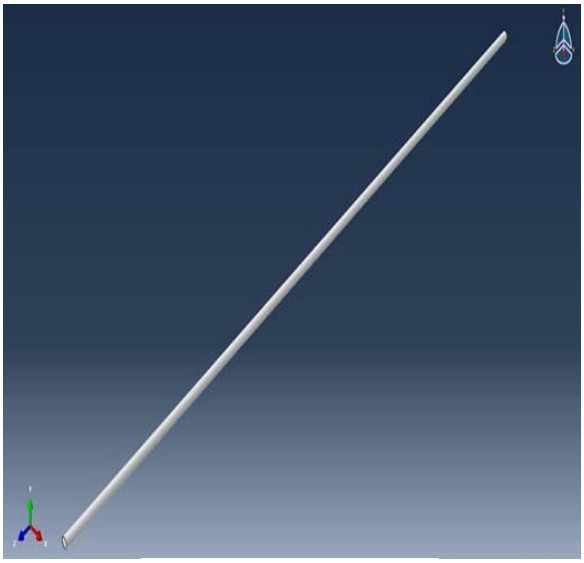

c) Steel Rebar

Figure 4.3: Model Components Created in ABAQUS

4.2.2 Defining Steps of Analysis

The static analysis has been conducted using the ABAQUS Standard code to numerically examine the behaviour of RC and RC encased in a PVC SIP forming system. ABAQUS Standard is ideal for static and quasi-static loadings where highly accurate stress solutions are required. The results with ABAQUS Standard can be used as the starting conditions for continuation in ABAQUS Explicit (Simulia 2011). This analysis ignores time-dependent material effects such as swelling, viscoelasticity and creep; however, it takes rate-dependent plasticity.

4.2.3 Boundary Conditions

Loading and boundary conditions were implemented in the model of all walls to simulate the experimental test setup, as shown in Figure 4.4. The symmetrical approach which has been used to simulate RC beams and PVC encased RC beams considers the $1/6^{th}$ of every full size beam by regarding its symmetrical condition. Along the planes of the symmetry, appropriate boundary conditions were applied. The symmetry boundary conditions were developed by inserting vertical restrains (rollers) at each node located in the planes of symmetry. Figure 4.4 demonstrates the appropriate boundary conditions used in this study.

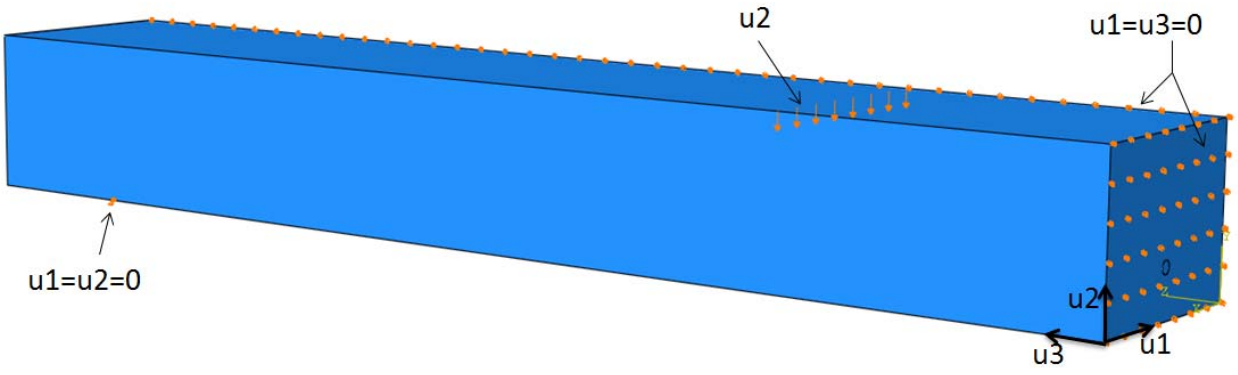

Figure 4.4: Boundary Conditions

At one end of the specimen, a roller support was produced by setting the allowable displacement, $U_1 = U_2 = 0$, and limiting movement in x and y directions. However, on the other faces of the specimen, a pin support was created by $U_1 = U_3 = 0$ to restrain the movement in x and z directions. The loading was applied as an imposed vertical displacement (U_2).

4.2.4 Meshing

The ABAQUS software package has plenty of techniques available to sub-divide the elements into tiny mesh elements. However, the most flexible technique is the free meshing technique. The first step in the free meshing technique is to determine the number of seeds. Using this option makes it feasible to distribute the seeds uniformly along the geometry. Figure 4.5 shows the meshing of the RC wall specimen.

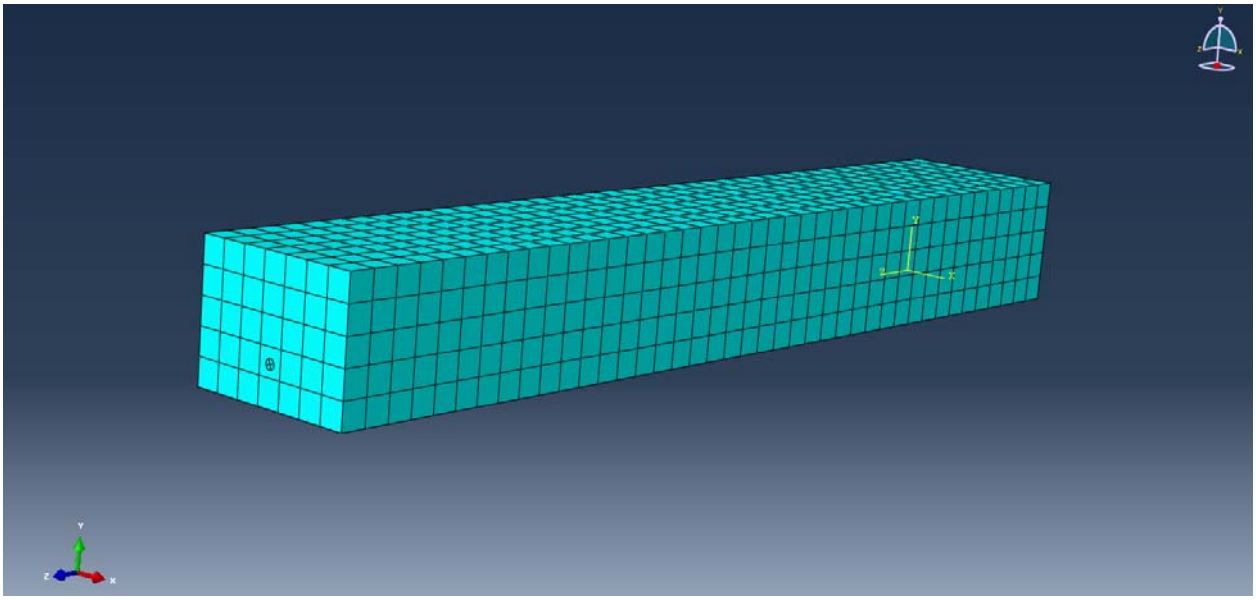

Figure 4.5: Meshing of the RC Wall Specimen

Element selection is very important in the mesh generation process. There are plenty of element types in the ABAQUS Standard library which could be used depending upon the specific request.

4.2.5 Selection of Elements

The wide range of 3D elements available in the elements library provides flexibility in modelling different geometries and structures. For each element, there are first or second order elements; first order elements have nodes only at the corner and use linear interpolation to calculate the necessary field variables such as displacements and temperatures. Second order elements have nodes in the middle, within the elements, and use quadratic interpolation rather than linear. First order elements were used for this study.

4.2.5.1 Three-dimensional Solid Elements

The main stress/displacement elements available in ABAQUS include the 4-node linear tetrahedron, the 6-node linear triangular prism, the 8-node linear brick, the 10-node quadratic tetrahedron, the 15-node quadratic triangle, and the 20-node quadratic brick. Each of these elements has three degrees of freedom per node.

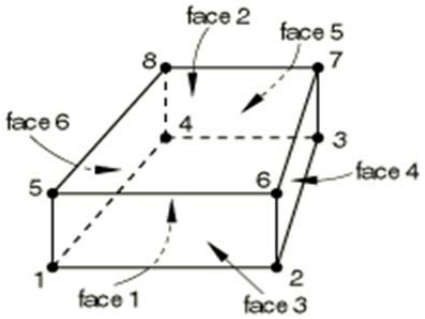

8-noded element (C3D8R)

Figure 4.6: ABAQUS Three-Dimensional Solid Elements (ABAQUS Documentation 2011)

Several studies (Anil and Ali 2009; Musharraf, et al. 2009) have previously used 8-noded, linear brick elements (C3D8R) in analyzing flexural problems similar to those considered in this study (Figure 4.6). According to ABAQUS (2011 manual), C3D8R with reduced integration scheme, is needed to adequately capture the flexural response of a beam. The hexahedral element (brick) exhibits potentially stiff behaviour with a slow convergence rate but prevents potential "mesh locking" when a reduced

integration analysis procedure is used. Moreover, hexahedral elements are shown to yield accurate results for linear and non-linear analysis involving contact, plasticity, and large deformations. Therefore, the C3D8R –type elements were used to model the concrete and steel rebar.

4.2.5.2 Shell Elements

ABAQUS has three-dimensional conventional, continuum, and axisymmetric shell elements. Triangular and quadrilateral conventional elements are available with linear interpolation and large strain or small strain formulation. The S4R elements were used to model the PVC SIP formwork, with reduced integration, membrane strain, and hourglass control scheme. S4R is a robust, general purpose element that is suitable for a wide range of applications. The S4R element uses a reduced integration rule with an integration point that makes the element computationally less expensive (Figure 4.7). The S4R element has several hourglass modes that may propagate over the mesh, uniformly reducing integration to avoid shear and membrane locking. The hourglass stabilization performs through an hourglass control parameter.

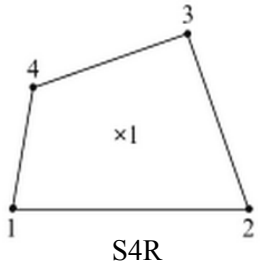

Figure 4.7: Reduced Integration Shell Element (Ellobody, 2014)

The reference surface of shell is defined by the shell element nodes and normal directions. The reference surface typically coincides with the shell's mid surface. However, many situations arise in which it is more convenient to define the reference surface as offset from the shell mid surface.

4.2.6 Contact between Elements

After assembling the components, the simulated components should be connected to each other. It is an important part in any type of FE analysis to model contact to simulate a proper interaction between the components. It is also important to define a suitable interaction between steel reinforcement and solid concrete beam. There are three alternative techniques for creating a proper bond between steel reinforcement and solid concrete elements in 3-D FE analysis. These techniques are classified as discrete, embedded, and smeared. In the case of discrete element modelling, steel reinforcement is modelled using truss or beam elements and establishing a connection with the concrete elements. This technique requires establishing common nodes between the concrete and steel elements. The embedded technique, on the other hand, regardless of establishing a mesh between the elements, can improve the simulation interaction between the concrete and reinforced steel. The Smeared technique is also an alternative method, where modelling might be used as composite layers (Tahmasebinia, 2008).

In the current investigation, the embedded technique was used to create a bond between solid concrete and steel reinforcement. The steel rebar is referred to as the “embedded region” and the concrete part is referred to as the “host region”. In this technique, the translational degree of freedom of the embedded part nodes becomes constrained to the value of the corresponding degree of freedom of the host part elements. Furthermore, the post failure stress-strain relationship for concrete subjected to tension is used, which accounts for tension stiffening, strain softening, and reinforcement (steel rebar) interaction with concrete. In the current investigation, the embedded constrain technique was also used to create the bond between the concrete and the PVC SIP forming system. The PVC SIP formwork part is referred to as the “embedded region” and the concrete part is referred to as the “host region”.

4.3 Model Validation

A model validation was performed to assess the validity of the CDP model for the concrete. For this purpose an RC control wall was used to validate the previously discussed FE parameters. The model

was verified by comparing its displacement behaviour and load carrying capacity to the experimental results.

In the current numerical analysis, the associated large deformation and the non-linearity made the convergence initially hard to achieve using the program default values. Therefore, to improve the convergence and to validate the model properly, very small increments were used (ABAQUS Documentation, 2012).

4.3.1 Dilation Angle (ψ)

Initially, the variation of parameter was performed on the dilation angle (ψ). The dilation angle (ψ) is the measure of the change in volumetric strain with respect to the change in shear strain (Figure 4.8). For a Mohr-Coulomb material like concrete, the value of the dilation angle varies between zero and the friction angle. Tuo (2008) recommended 30° for concrete material. Lee and Fenves (1998) also proposed a dilation angle of 30° for both uniaxial compression and tension.

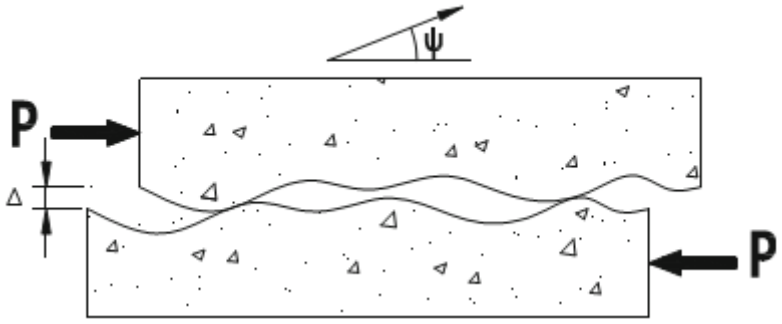

Figure 4.8: Dilation Angle (Ren, 2014)

From Figure 4.9 it can be seen that, as the dilation angle increased, the displacement capacity, yield load and peak load significantly increased. A dilation angle of 30° was used for this study based on the results of the dilation angle validation after fixing all other parameters (stress-strain curves for concrete, steel and PVC).

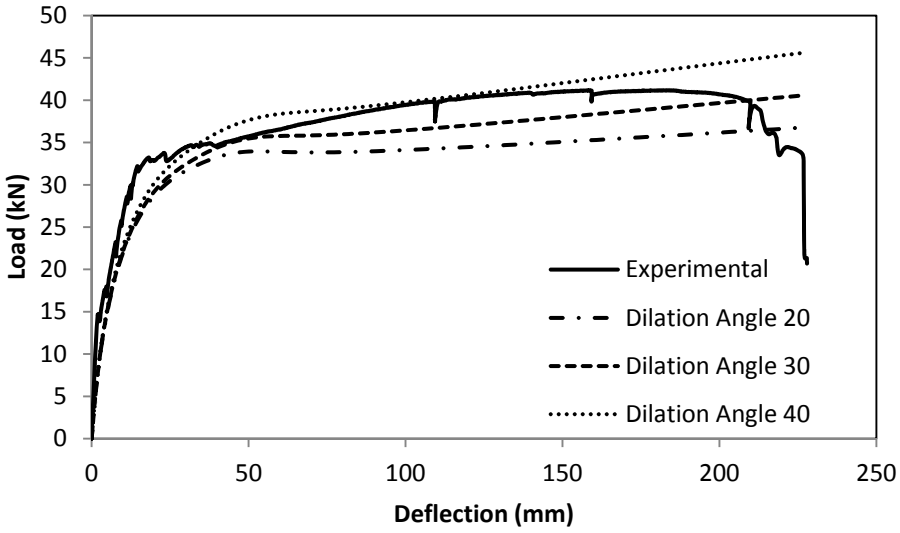

Figure 4.9: Validation of Dilation Angle (C-10M-152mm)

4.3.2 Mesh Sensitivity Analysis

In order to provide an FE analysis with reasonably accurate results, the effectiveness of mesh density was checked by conducting a mesh sensitivity analysis. For this purpose, the mesh can be changed by changing the size of the seeds in the developed model. However, refining the mesh elements can increase computational costs. The results of different mesh sizes of the RC wall are presented in Figure 4.10. The results with 30mm seed size are reasonably close to the results obtained from other experiments.

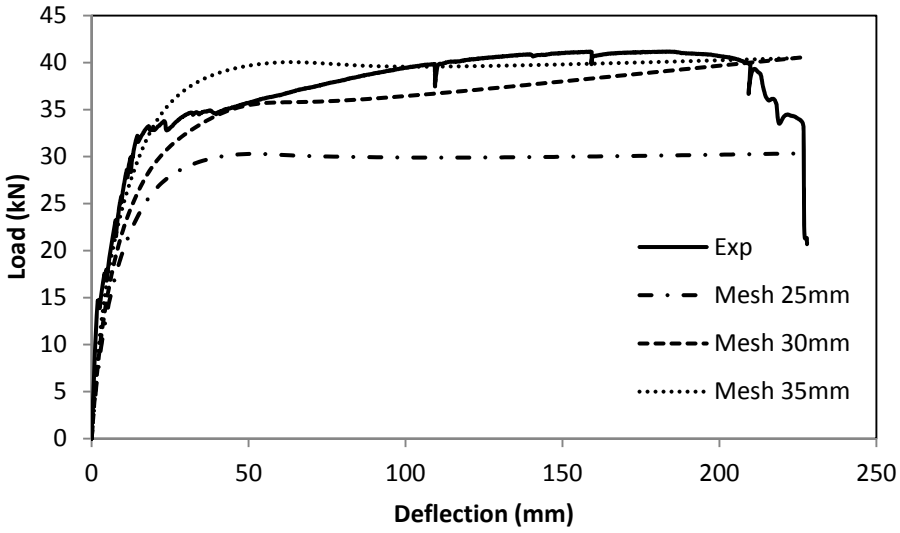

Figure 4.10: Mesh sensitivity Analysis of FE Model of Control Wall (C-10M-152mm)

4.4 Study Parameters

This study was carried out through the development of 42 models to investigate the thickness of RC walls with and without PVC encasement, reinforced steel ratio, concrete compressive strength (f_c'), thickness of PVC SIP formwork, and strength of the PVC used in formwork. The main study consisted of three main groups control walls (RC walls without PVC encasement), PVC encased RC walls with flat panels, and PVC encased RC walls with hollow panels. Table 4-1 shows the matrix of the main study with some additional parameters shown in Table 4-2.

Table 4-1: Main Study

Type	Parameters					
	Thickness (mm)	Reinforcement Ratio -	Concrete Compressive Strength (f_c') (MPa)			
Control Walls	152	0.00454	20	22.5	25	30
	178	0.00366	20	22.5	25	30
	203	0.00309	20	22.5	25	30
PVC Encased Walls with Flat Panel	152	0.00443	20	22.5	25	30
	178	0.00358	20	22.5	25	30
	203	0.00303	20	22.5	25	30
PVC Encased Walls with Hollow Panel	152	0.00398	20	22.5	25	30
	178	0.00327	20	22.5	25	30
	203	0.00279	20	22.5	25	30

Table 4-2: Additional Parameters

Concrete Compressive Strength (f_c')	22.5 MPa
Wall	PF-10M-178 mm
Thickness of PVC SIP Formwork	t = 1.5 mm
	t = 3.0 mm
	t = 6.0 mm
Strength of PVC used in Formwork	30% decrease
	Actual
	30% increase

Chapter 5: Results and Discussion

In this Chapter, the numerical model results from the control specimens and PVC encased specimens are presented and compared. The results included the general behaviour of numerical models, load versus deflection curves, and load versus strain behaviour of the different components of the walls.

5.1 Behaviour of the Control RC Walls

5.1.1 Load-Deflection

The typical load versus deflection behaviour of RC walls is presented in Figure 5.1. The vertical axis represents the applied load (kN) and the horizontal axis represents the deflection (mm). The FE and experimental results showed that the load versus deflection behaviour can be defined into three distinct phases: un-cracked, cracked, and post yield. The un-cracked phase refers to the rapid rise in load. The cracked phase occurs when the load increases linearly with deflection between the cracking and yield load (load at which steel rebar yields). In this phase, stiffness decreases as compared to the un-cracked phase. After yield load, the post yield phase starts where the deflection increases rapidly with little increase in load.

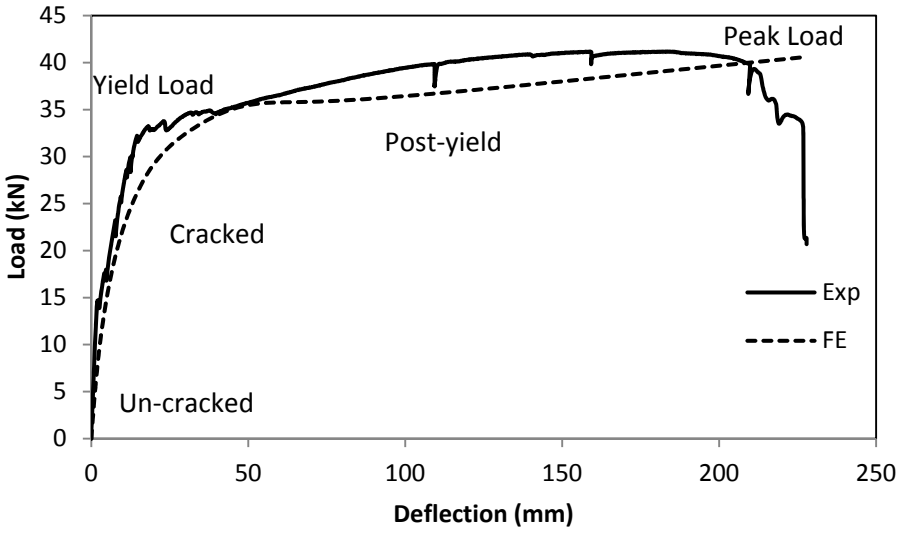

Figure 5.1: Load vs Deflection Curve of 152 mm thick RC Wall

5.1.1.1 Effect of Concrete Core Thickness

Table 5-1 presents a comparison between experimental and FEM results for RC control walls for the three wall thicknesses (152, 178 and 203 mm). The yield loads, peak loads and their corresponding deflections are presented. The yield and peak loads of the specimens increased as the concrete core thickness increased. The experimental specimens with a core thickness of 152 mm (6 inches) showed yield and peak loads of 32 kN and 41 kN, respectively, while FEM results were 28.5kN and 40.5 kN for the yield and peak loads, respectively. Therefore, the differences were 11% for the yield load and 1% for the peak load. As the concrete core thickness increased to 178 mm (7 inches), the yield and peak loads of the FEM increased to 43.3 kN and 55.6 kN with a respective error of 3% and 0.5%. The RC wall with a core thickness of 203 mm (8 inches) showed a yield load of 52 kN and a peak load of 66 kN, with an error of 2% and 7%, respectively. Overall, the FEM results are in good agreement with the experimental results.

At the yield load, the deflection was decreased as a result of an increase in concrete core thickness. The yield deflection was 18.4 mm for the 152 mm thick RC wall, 18.3 mm for 178 mm thick RC wall, and 14.1 mm for the 203 mm thick RC wall, while the ultimate deflection was 223 mm for the 152 mm thick RC wall, 138 mm for 178 mm thick RC wall, and 133 mm for 203 mm thick RC wall.

Table 5-1: Control Wall Results Comparison

P_{yield} (kN)		Error %	P_{peak} (kN)		Error %	Δ_{yield} (mm)		$\Delta_{ultimate}$ (mm)	
Exp	**FE**		**Exp**	**FE**		**Exp**	**FE**	**Exp**	**FE**
Thickness = 152 mm (6 inch)									
32	28.5	-12	41	40.5	-1	14.4	18.4	226	223
Thickness = 178 mm (7 inch)									
44.5	43.3	-3	55.5	55.6	0.5	11.4	18.3	139	138
Thickness = 203 mm (8 inch)									
53	52	-2	66	70.8	7	10.1	14.1	136	133

*: Δ stands for deflection

Figure 5.2 presents the effect of thickness on RC walls.

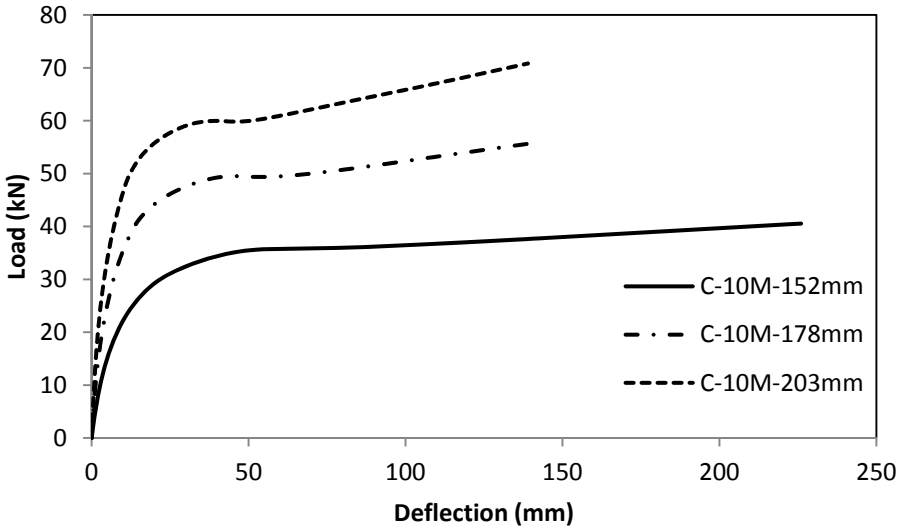

Figure 5.2: Load vs Deflection Curves for RC Walls with Different Core Thickness

5.1.2 Load-Strain

The strain values of tension steel rebar as estimated by the model were also compared with the experimental strain values recorded during testing. The typical load versus strain behaviour of RC wall is presented in Figure 5.3. The horizontal axis represents the steel strain and the vertical axis represents the applied load (kN). Moreover, positive values indicate tensile strain. The strain increased linearly with the applied load until the load reached the yield point. After yielding, the strain increased rapidly with a small increase in the applied load.

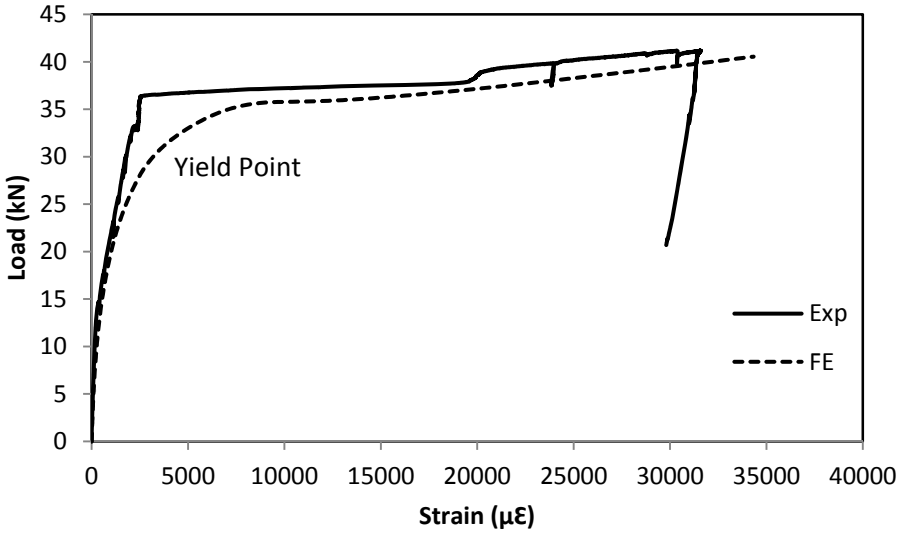

Figure 5.3: Load vs Steel Strain of 152mm Thick RC Wall

Table 5-2 presents the steel rebar strain comparison between experimental and FEM results. The steel strain value of the FE model was 31401$\mu\varepsilon$ for 152 mm thick RC wall with very little difference from the experimental work. The strain values were 23181$\mu\varepsilon$, and 26231$\mu\varepsilon$ for 178 mm and 203 mm thick RC walls, respectively. Overall, the calculated strains values are in good agreement with the experimental results.

Table 5-2: Steel Rebar Strain Comparison between Experimental and FEM Results

Steel Rebar Strain ($\mu\varepsilon$)				
Wall	Experimental	FE Model	Difference	Error
C-10M-152mm	31403	31401	2	-0.00%
C-10M-178mm	23181	23869	688	0.03%
C-10M-203mm	26231	26687	456	0.02%

5.2 Behaviour of RC Walls Encased in PVC Flat Panels

5.2.1 Load Deflection

All the FEMs had almost similar load versus deflection behaviour. Figure 5.4 shows a typical load versus deflection curve for flat panels PVC encased RC walls. The horizontal axis represents the mid-span deflection (mm) and the vertical axis represents the applied load (kN). Before yielding, the load increased linearly with the increase of deflection. Past the yield point, the deflection increased rapidly as compared to the applied load. The flat panel models showed a significant improvement in yield load and ductility. In general, the predicted load-deflection curve showed similar behaviour except at failure. One possible reason for this difference may be related to the bond between PVC and concrete. In FE modelling a perfect bond was assumed in contrast to the minor bond slip behaviour observed in experiments.

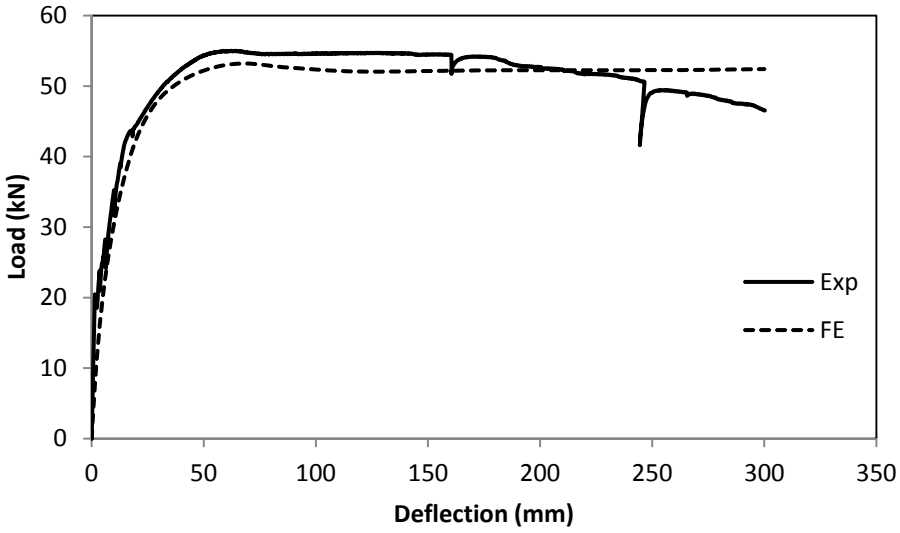

Figure 5.4: Load vs Deflection of 152mm Thick RC Wall Encased in PVC Flat Panels

5.2.1.1 Effect of Concrete Core Thickness

Table 5-3 presents the comparison between experimental and FEM results for RC walls encased with PVC flat panels. It provides the information about yield loads, peak loads, and their corresponding deflections. Moreover, it also provides the percentile improvement in yield load, peak load, and ultimate deflection due to the use of PVC SIP formwork.

PVC encased RC walls with flat panels showed a higher yield load than the equivalent RC wall models. The yield loads for the PVC encased RC walls were 41.3 kN, 49 kN, and 59.9 kN for the 152 mm, 178 mm, and 203 mm thick walls, respectively. This shows an increase in yield load of 44%, 13%, and 15% for the 152 mm, 178 mm, and 203 mm thick walls, respectively, in comparison to the equivalent RC wall models without PVC. This improvement can be attributed to the PVC panel on the tension side of the wall providing a supplementary tensile force reinforcement within the cross section. At the yield load, the deflection decreased as a result of an increase in concrete core thickness. The yield deflection was 18.5 mm for the 152 mm thickness, 13.2 mm for 178 mm thickness, and 10.9 mm for 203 mm

thickness. Therefore, the presence of the PVC panels did not have a significant influence on the yield deflection.

The PVC encased RC walls with flat panels showed an increase in the peak load over the control RC wall models without PVC. The peak loads for the PVC encased RC wall models were 52.4 kN, 73.6 kN, and 90.3 kN for the 152 mm, 178 mm, and 203 mm thick walls, respectively. This represents an increase of 29%, 32%, and 28% for the 152 mm, 178 mm, and 203 mm thick walls, respectively. The ultimate deflection was 295 mm, 259 mm, and 259 mm for PVC encased RC walls with 152 mm, 178 mm, and 203 mm core thickness, respectively. Therefore, it was a significant 32% to 95% improvement in the ultimate deflection as compared to the RC wall models.

Table 5-3: PVC Encased RC Wall with Flat Panel Results Comparison

P_{yield} (kN)		Error %	P_{peak} (kN)		Error %	Δ_{yield} (mm)		$\Delta_{ultimate}$ (mm)	
Exp	**FE**		**Exp**	**FE**		**Exp**	**FE**	**Exp**	**FE**
Thickness = 152 mm									
43	41.3	-4	55	52.4	-5	15.4	18.5	300	295
Improvement									
34%	44%	-	34%	29%	-	-	-	33%	32%
Thickness = 178 mm									
54	49.0	-10	72	73.6	2	9.8	13.2	255	253
Improvement									
21%	13%	-	30%	32%	-	-	-	83%	83%
Thickness = 203 mm									
64	59.9	-7	89	90.3	1.5	8.2	10.9	262	259
Improvement									
21%	15%	-	35%	28%	-	-	-	93%	95%

*: Δ stands for deflection

Figure 5.5 presents the effect of thickness on PVC encased RC walls with flat panels.

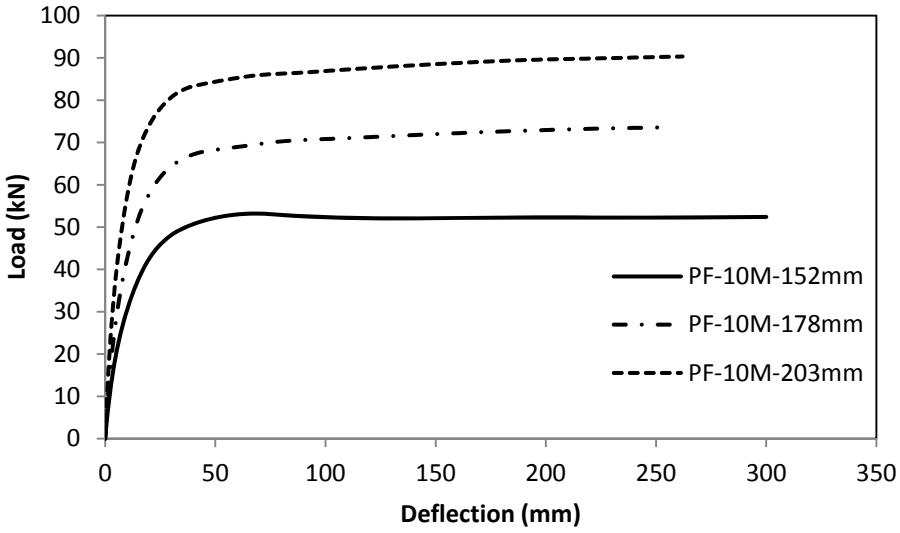

Figure 5.5: Load vs Deflection Behaviour of RC Walls Encased with PVC Flat Panels

5.2.2 Load versus Strain

The strain in the tension PVC panel (ε_{pvc}) as estimated by the model is compared with the experimental strain values recorded during testing. The typical load versus PVC panel strain behaviour is presented in Figure 5.6.The horizontal axis represents the PVC strain and the vertical axis represents the applied load (kN). The strain increased linearly with the applied load until the load reached the yield point. After yielding, the strain value increased rapidly with a small increase in the applied load.

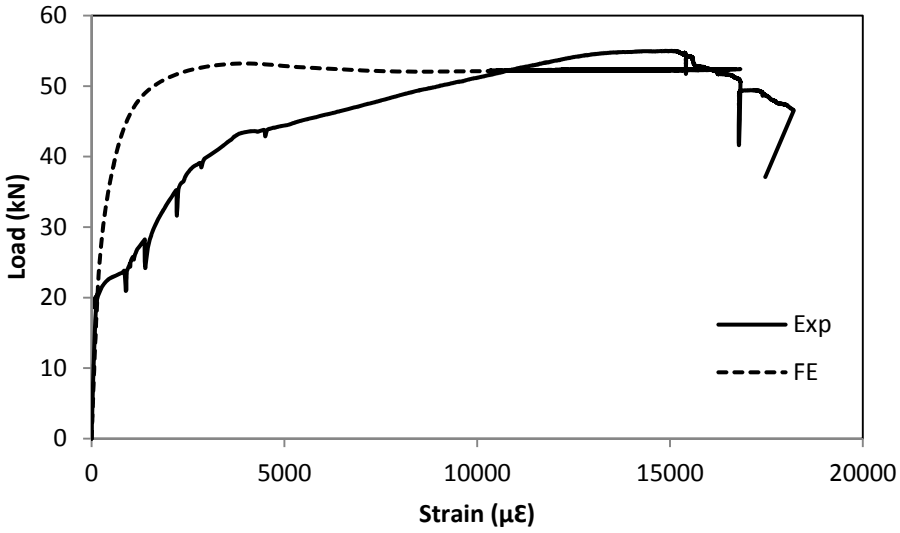

Figure 5.6: Load vs PVC Panel Strain Curve for PF-10M-152 mm Thick Wall

Table 5-4 presents the PVC panel strain comparison between experimental and FEM results at peak load. The PVC panel strain value of FEM was 16800$\mu\varepsilon$ for 152 mm thick wall with an error difference of 7% from the experimental work. However, the difference was 26% for the 178 mm thick wall. The values of PVC panel strains were 24600$\mu\varepsilon$ and 30300$\mu\varepsilon$ for 178 mm and 203 mm thick walls, respectively. The calculated strain values are in good agreement with the experimental results.

Table 5-4: PVC Panels Strain Comparison Between Experimental and FEM Results

PVC Panels Strain ($\mu\varepsilon$)				
Wall	Experimental	FE Model	Difference	Error
PF-10M-152mm	18000	16800	1200	7%
PF-10M-178mm	31000	24600	6400	26%
PF-10M-203mm	N/A	30300	N/A	N/A

5.3 Behaviour of RC Walls Encased in PVC Hollow Panels

5.3.1 Load versus Deflection

Figure 5.7 shows a typical load versus deflection curve for PVC encased RC walls with hollow panels. The horizontal axis represents the mid-span deflection (mm) and the vertical axis represents the applied load (kN). Before yielding, the load increased linearly with the increase of deflection. Past the yield point, the deflection increased rapidly as compared to the applied load. The hollow panel models showed a significant improvement in the yield load and ductility as similar to the flat panel encased walls. The predicted load-deflection curve showed a similar behaviour for the first two stages (un-cracked and cracked). However, in the post-yield region the FEM results were quite smooth when compared to the jagged behaviour observed in the experimental results. This difference could be attributed to the assumed bond behaviour (perfect bond) between concrete and PVC in comparison to the experimentally observed bond slip behaviour between concrete and PVC.

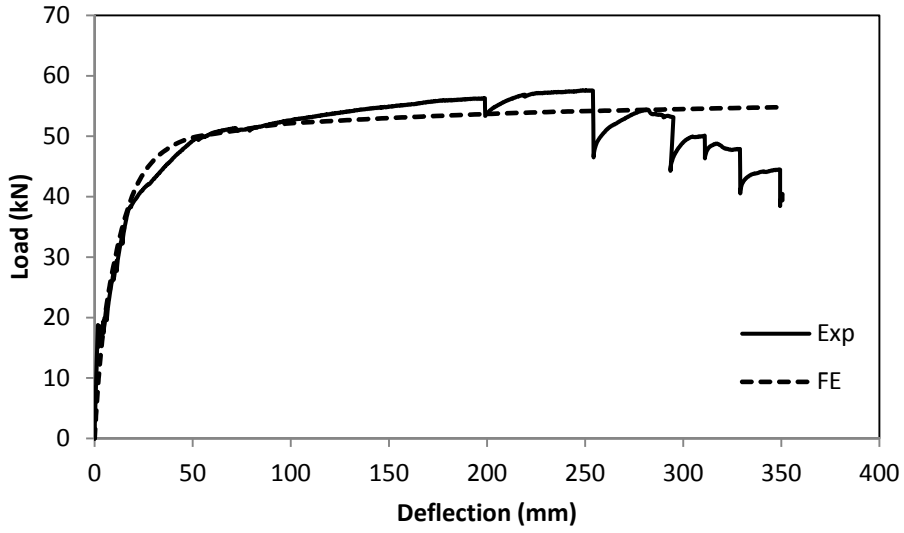

Figure 5.7: Load vs Deflection of 152mm Thick RC Wall Encased with PVC Hollow Panels

5.3.1.1 Effect of Concrete Core Thickness

Table 5-5 presents a comparison between experimental and FEM results for the RC walls encased with PVC hollow panels. It provides the information about yield loads, peak loads, and their corresponding deflections. Moreover, it also provides the percentile improvement in yield load, peak load, and ultimate deflection due to the use of the PVC SIP formwork.

Similar to the walls with flat panels, PVC encased RC walls with hollow panels showed a higher yield load than the equivalent RC wall models. The yield load increased as the concrete core thickness increased. The yield loads for the PVC encased RC walls with hollow panels were 39.9 kN, 45 kN, and 59.7 kN for the 152 mm, 178 mm, and 203 mm thick walls, respectively. In comparison to the equivalent RC wall models, these results showed yield load improvements of 25%, 1%, and 13% for the 152 mm, 178 mm, and 203 mm thick walls, respectively. This improvement was due to the PVC panel in tension providing additional tensile force reinforcement to the wall cross-section. At the yield load, the deflection decreased as a result of an increase in concrete core thickness. The yield deflection was 18.9 mm for the 152 mm thick PVC encased RC wall, 18.8 mm for 178 mm thick PVC encased RC wall, and 13.3 mm for 203 mm thick PVC encased RC wall. Therefore, the presence of the PVC panels did not have a significant influence on the yield deflection.

The PVC encased RC walls with hollow panels showed an increase in the peak load over the control RC wall models. The peak loads for the PVC encased RC wall models were 54.8 kN, 56 kN, and 81 kN for the 152 mm, 178 mm, and 203 mm thick walls, respectively. This showed a peak load improvement of 34%, 1%, and 23% for the 152 mm, 178 mm, and 203 mm thick walls, respectively, in comparison to the control walls. The ultimate deflection was 350 mm, 155 mm, and 214 mm for PVC encased RC walls with 152 mm, 178 mm, and 203 mm core thickness, respectively. Therefore, there was a significant improvement in ultimate deflection as compared to the RC wall models. The increase in the ultimate deflection varied between 55% and 57% as shown in Table 5-5.

Table 5-5: PVC Encased RC Wall with Hollow Panel Results

P_{yield} (kN)		Error %	P_{peak} (kN)		Error %	Δ_{yield} (mm)		$\Delta_{ultimate}$ (mm)	
Exp	**FE**		**Exp**	**FE**		**Exp**	**FE**	**Exp**	**FE**
Thickness = 152 mm (6 inch)									
38	39.9	5	57	54.8	-3	17.6	18.9	311	350
Improvement									
19%	25%	-	39%	34%	-	-	-	38%	55%
Thickness = 178 mm (7 inch)									
46	45.0	-2	75	56.0	-23	14.6	18.8	143	155
Improvement									
3%	1%	-	35%	1%	-	-	-	3%	12%
Thickness = 203 mm (8 inch)									
60	59.7	-1	95	81	-15	9.6	13.3	216	214
Improvement									
13%	13%	-	44%	23%	-	-	-	59%	57%

*: Δ stands for deflection

Figure 5.8 presents the effect of thickness on RC wall encased with PVC hollow panels.

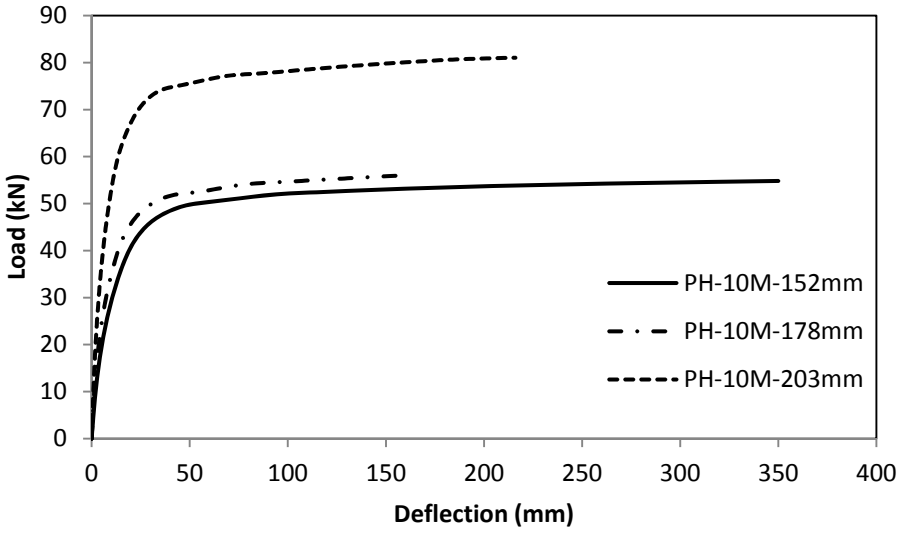

Figure 5.8: Load vs Deflection Behaviour of RC Walls Encased with PVC Hollow Panels

5.4 Comparison between FEM and Experimental Yield Loads

In the flexural behaviour of RC members, the yield load is considered to be the most important parameter. Therefore a separate detailed comparison between FEM and experimental yield loads is presented in Table 5-6 and Figure 5.9. The FEM values for control wall specimens were consistently underestimated with the model exceeding the test results by an average of 6% (12% maximum for only one model). However, the results of the PVC encased specimens were underestimated by an average of 5% (10% maximum for one model).

Table 5-6: Summary of Experimental vs FEM Yield Load

		Yield Load		
	Specimen	**Experimental (kN)**	**FE Model (kN)**	**Error (%)**
Control	C-6-10	32	28.51	-12.2%
	C-7-10	44.5	43.35	-2.7%
	C-8-10	53	51.96	-2.0%
Flat Panel	PF-6-10	43	41.31	-4.1%
	PF-7-10	54	49.02	-10.2%
	PF-8-10	64	59.90	-6.8%
Hollow Panel	PH-6-10	38	39.86	5%
	PH-7-10	46	44.96	-2.3%
	PH-8-10	60	59.72	-0.5%

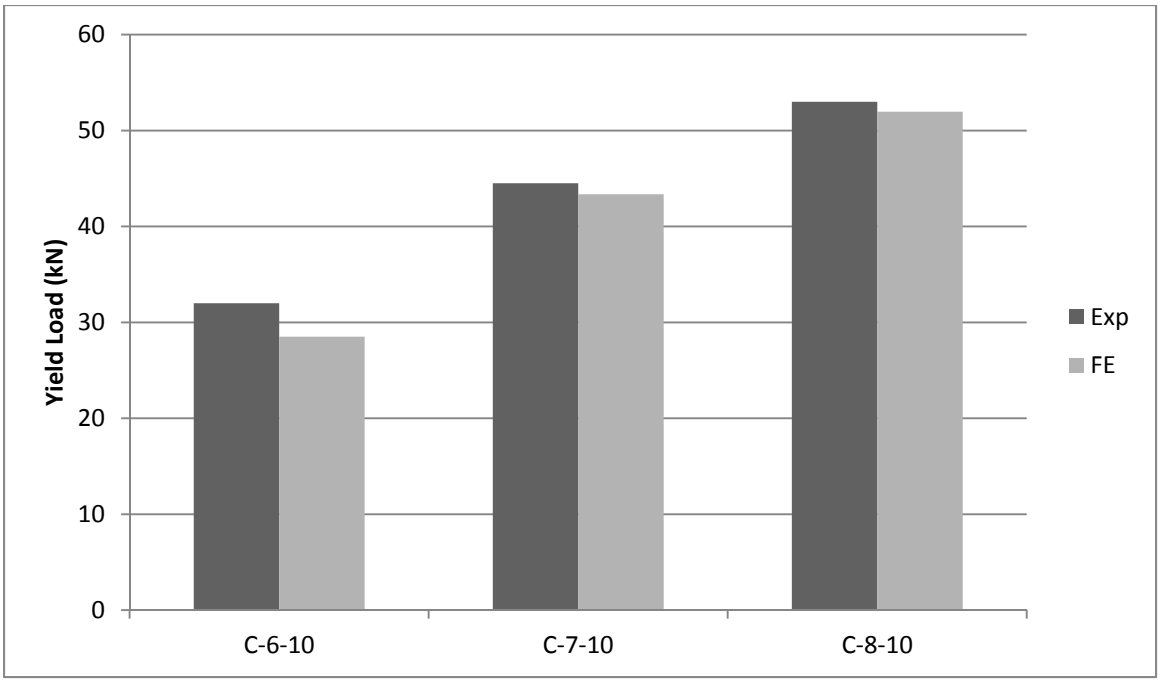

a) Control Walls

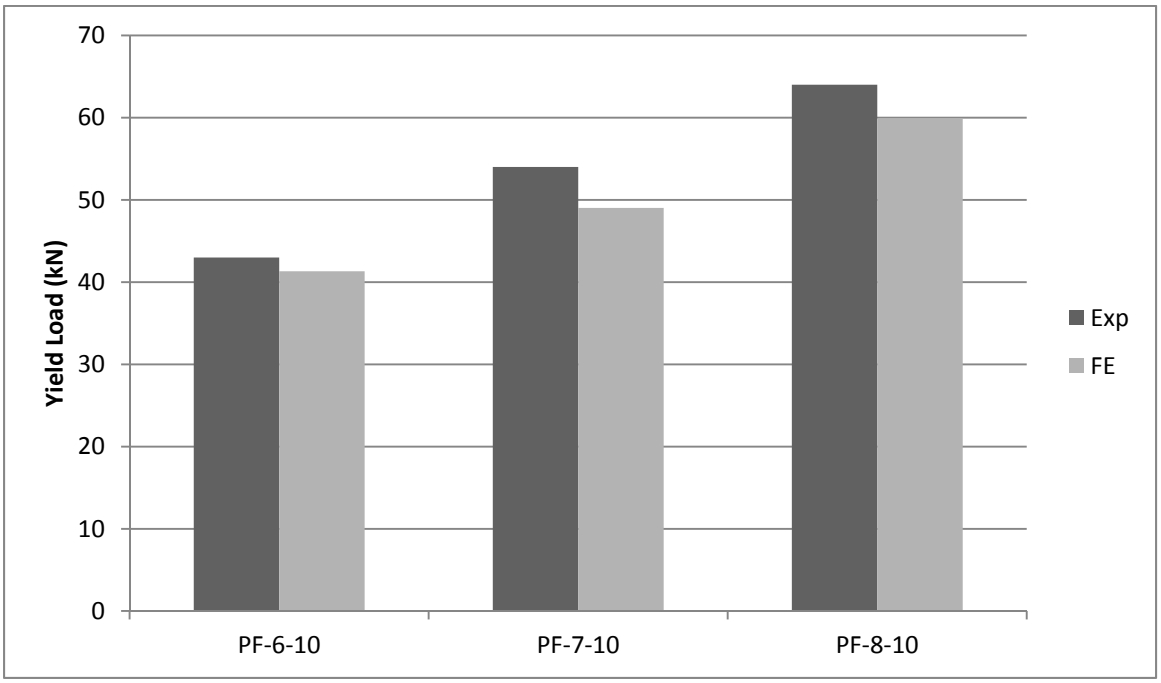

b) PVC Encased Walls with Flat Panels

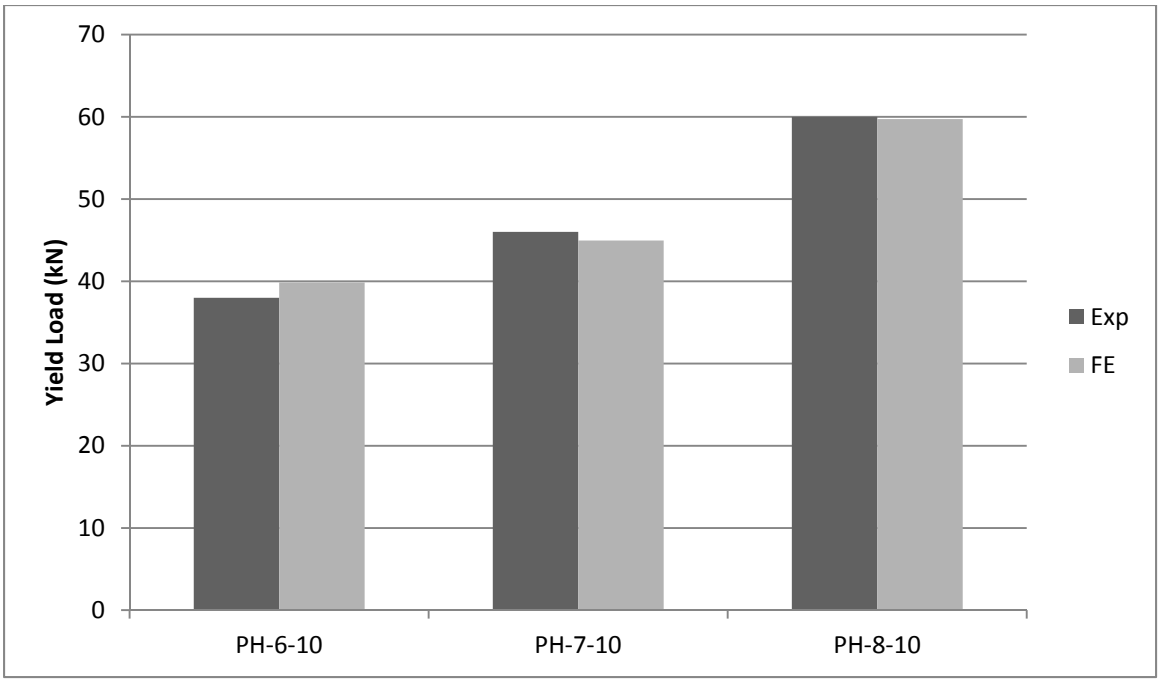

c) PVC Encased Walls with Hollow Panels

Figure 5.9: Experimental versus FEM Yield Loads

5.5 Comparison between FEM and Experimental Peak Loads

Table 5-7 and Figure 5.10 compare the experimental peak load results with the FEM results. The FEM values for control wall specimens are in agreement with the test results. FEMs only had a maximum difference of 7% in one model. The peak loads of FEM with flat panels are in good agreement (within ±4.7%) with the test results. However, the results of the PVC encased models with hollow panels were underestimated by 22% and 15% for 152 mm and 178 mm core thickness of concrete, respectively. The model is overestimated for one specimen in particular, PH-8-10. The peak load of this wall is estimated 3% greater than the experimental results.

Table 5-7: Summary of Experimental vs FE Model Peak Load

		Peak Load		
	Specimen	**Experimental (kN)**	**FE Model (kN)**	**Error (%)**
Control	C-6-10	41	40.54	-1.0%
	C-7-10	55.5	55.63	0.5%
	C-8-10	66	70.81	7.3%
Flat Panel	PF-6-10	55	52.41	-4.7%
	PF-7-10	75.3	73.59	-2.27%
	PF-8-10	89	90.33	1.47%
Hollow Panel	PH-6-10	57	58.81	-3.07%
	PH-7-10	72	55.93	22.3%
	PH-8-10	95	81.04	14.7%

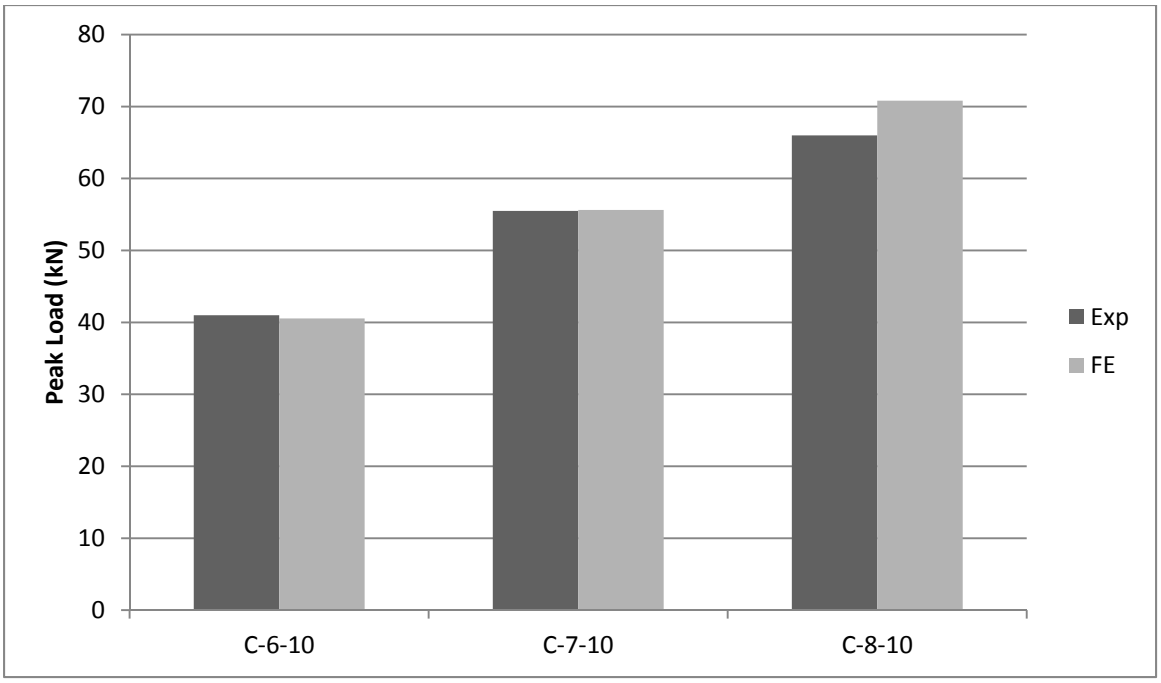

a) Control Wall

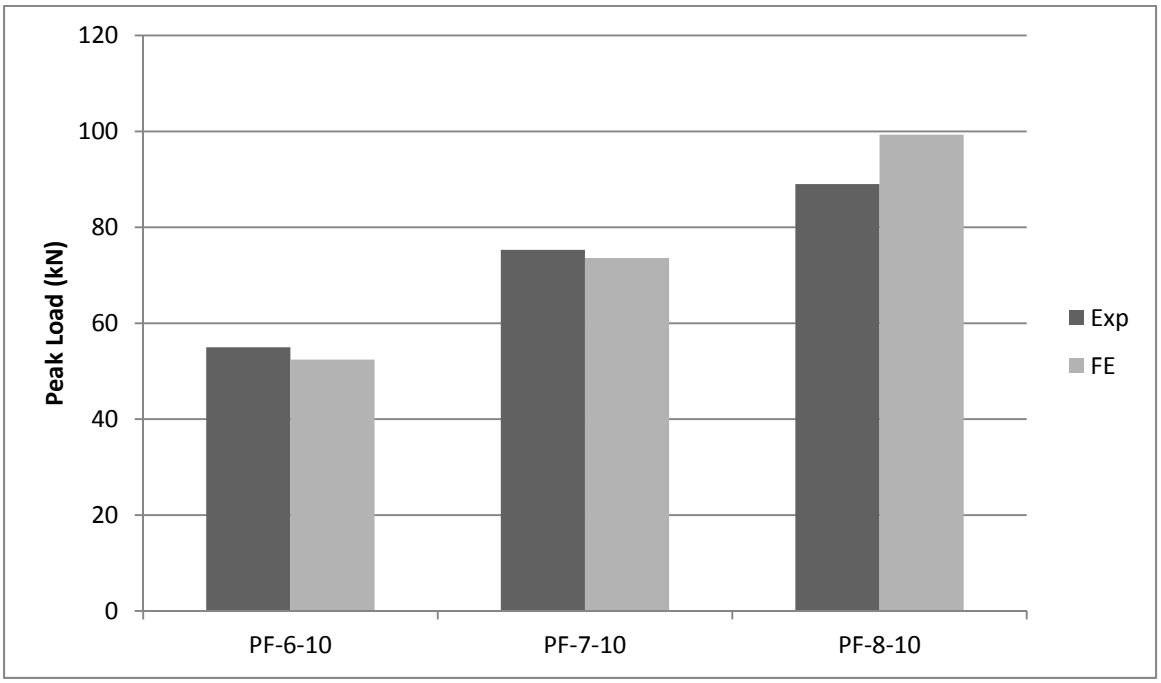

b) PVC Encased Walls with Flat Panels

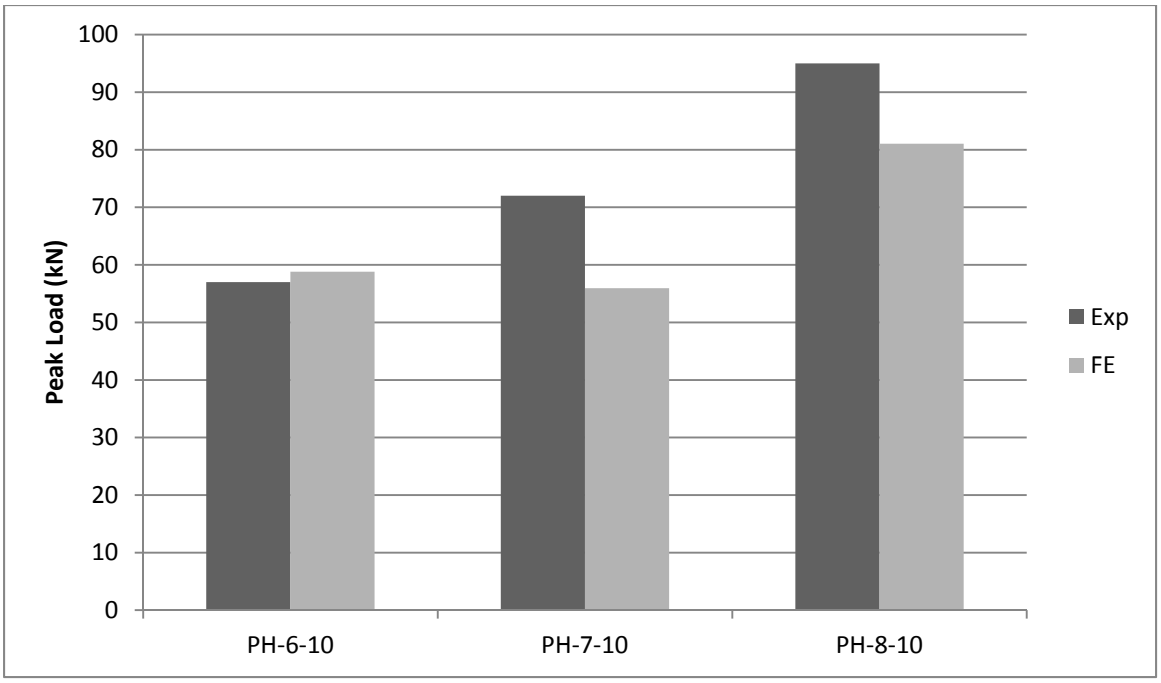

c) PVC Encased Walls with Hollow Panels

Figure 5.10: Experimental versus FEM Peak Loads

5.6 Summary

From the FE analysis, the load carrying capacity, deflection, and ductility were investigated. The strains of steel and PVC panels were also studied. The PVC SIP formwork enhanced the load carrying capacity and ductility. The FEM results were found to be in good agreement with the test results, with an average error of 5.67%, 7.03%, and 2.6% in the yield loads for the simple RC walls, RC walls encased with PVC flat panels, and RC walls with PVC hollow panels, respectively. The error for peak load was 3%, 3.35%, and 13.3% for the simple RC walls, RC walls encased with PVC flat panels, and RC walls with PVC hollow panels, respectively.

Chapter 6: Parametric Study

6.1 General

A parametric study was conducted to investigate the factors that may affect the behaviour of PVC encased RC walls. The factors studied included: concrete strength (f_c'), thickness of PVC formwork, and strength of PVC used in formwork. All analytical models (for RC control wall and RC walls encased with PVC flat panels) presented up to this point were utilized for this study. The main objective of the parametric study was to provide an in-depth understanding of the PVC SIP formwork for future design consideration of the PVC panels. The following sections present and discuss the results of the parametric study.

6.2 Effect of Concrete Compressive Strength

6.2.1 RC Walls without PVC SIP Formwork

A parametric study was conducted to investigate the effect of concrete compressive strength (f_c') on the performance of the walls using four values of f_c' ; 20 MPa, 22.5 MPa, 25 MPa, and 30 MPa. Increasing the concrete compressive strength by 12.5% (from 20MPa to 22.5MPa) increased the yield load by 15.5%, 28%, and 17%, respectively for RC walls with a core thickness of 152mm, 178mm, and 203mm. Increasing the concrete compressive strength again by 12.5% (from 22.5MPa to 25MPa), increased the yield load by 3.1%, 1%, and 11.8%, respectively, for RC walls with a core thickness of 152mm, 178mm, and 203mm. Increasing the concrete compressive strength by 25% (from 25MPa to 30MPa), increased the yield load by 12.9%, 5.25%, and 14%, respectively for RC walls with a core thickness of 152mm, 178mm, and 203mm. Figure 6.1 presents the change in yield load with various concrete compressive strengths.

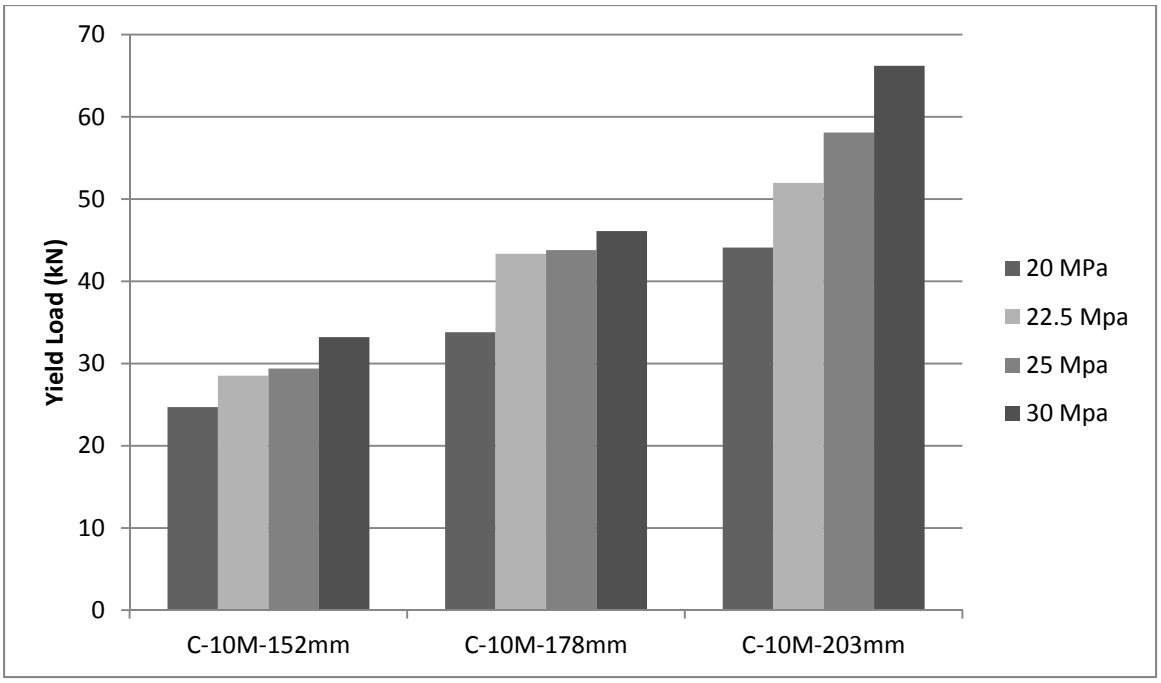

Figure 6.1: Change in Yield Load with Variation in Concrete Compressive Strength for Simple RC Walls

Moreover, increasing the concrete compressive strength by 12.5% from 20MPa to 22.5MPa increased the peak load by 10.5%, 8.4%, and 8.6%, respectively, for RC walls with a core thickness of 152mm, 178mm, and 203mm. Increasing the concrete compressive strength by 12.5% from 22.5MPa to 25MPa increased the peak load by 6.3%, 7.3%, and 17.8%, respectively, for RC walls with a core thickness of 152mm, 178mm, and 203mm. Increasing the concrete compressive strength from 25MPa to 30MPa again, an increase of 25% increased the peak load by 13.5%, 12.4%, and 11.7%, respectively, for RC walls with core thickness of 152mm, 178mm, and 203mm. Figure 6.2 presents the change in peak load with variation in concrete compressive strength.

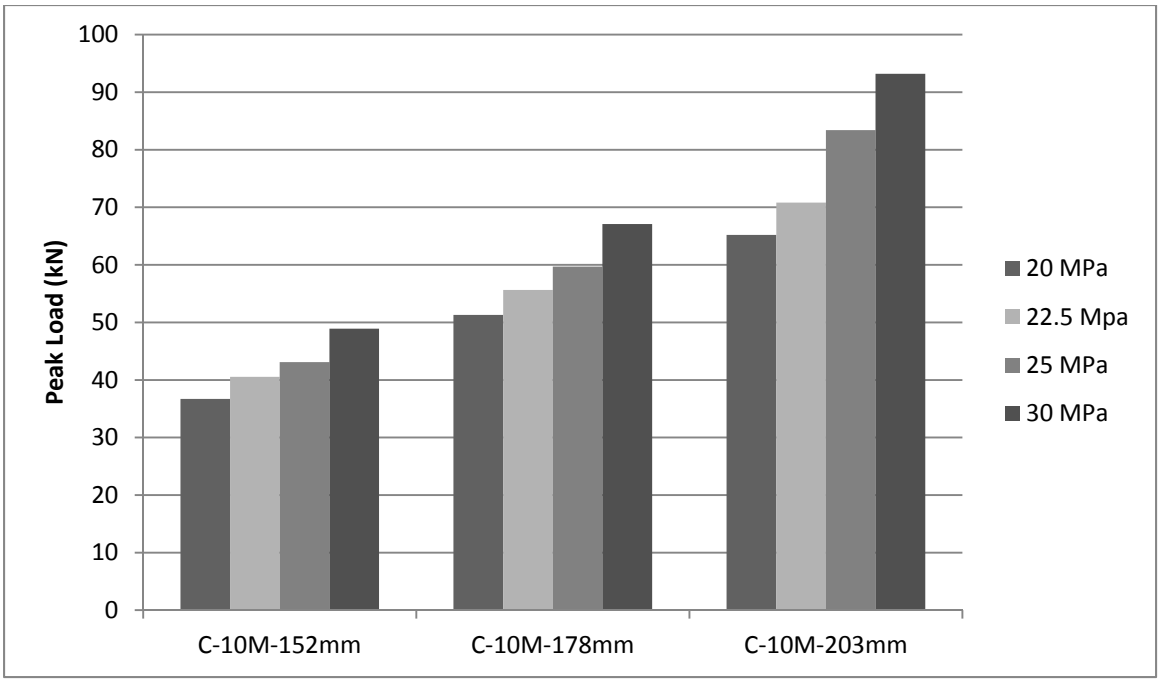

Figure 6.2: Change in Peak Load with Variation in Concrete Compressive Strength for Simple RC Walls

6.2.2 RC Walls Encased with PVC SIP Formwork

In RC walls with PVC SIP formwork, the increase in yield and peak loads were very much consistent with the increase in the core thickness of the walls. An increase in the concrete compressive strength of 12.5% from 20MPa to 22.5MPa increased the yield load by 14.4%, 5.4%, and 5.3%, respectively, for PVC encased RC walls with core thickness of 152mm, 178mm, and 203mm. Increasing the concrete compressive strength again by 12.5% from 22.5MPa to 25MPa increased the yield load by 4.8%, 13.6%, and 14.9%, respectively, for PVC encased RC walls with core thickness of 152mm, 178mm, and 203mm. Increasing the concrete compressive strength by 25% from 25MPa to 30MPa increased the yield load by 10.7%, 14.7%, and 15.1%, respectively, for RC walls with core thickness of 152mm, 178mm, and 203mm. Figure 6.3 presents the change in yield load with variation in concrete compressive strength.

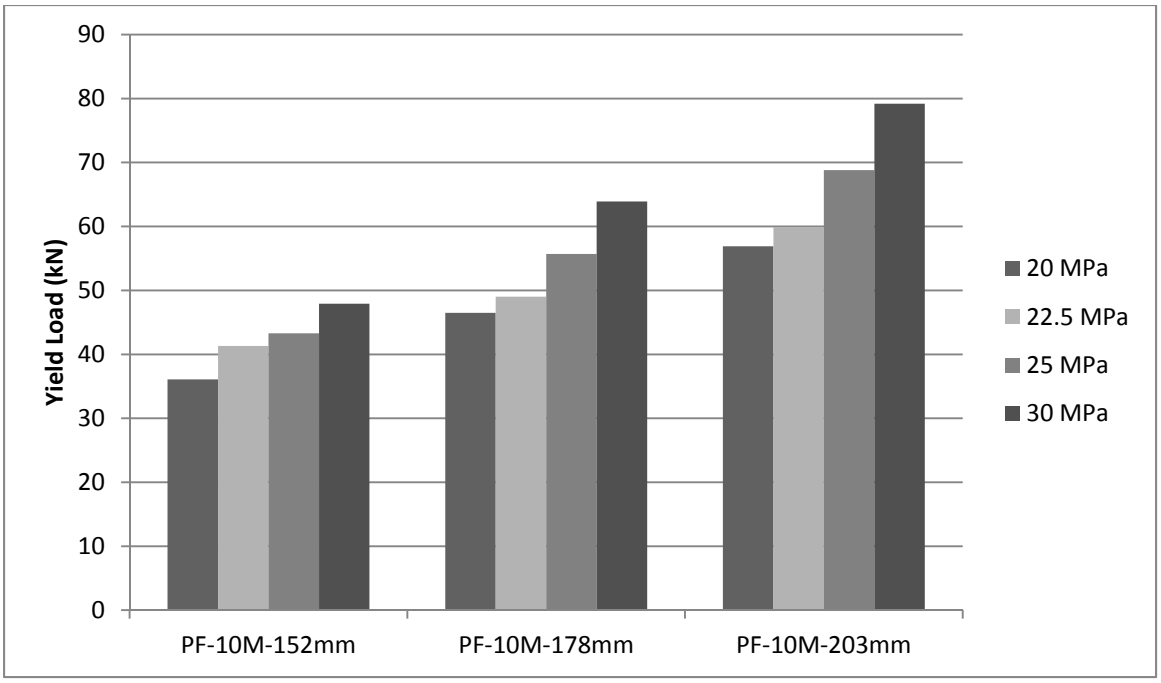

Figure 6.3: Change in Yield Load with Variation in Concrete Compressive Strength for PVC Encased RC Walls

Moreover, increasing the concrete compressive strength by 12.5% from 20 MPa to 22.5 MPa increased the peak load by 4.8%, 6.5%, and 6.8%, respectively, for PVC encased RC walls with core thickness of 152mm, 178mm, and 203mm. Increasing the concrete compressive strength again by 12.5% from 22.5MPa to 25MPa increased the peak load by 7.4%, 5.3%, and 5.6%, respectively for PVC encased RC walls with core thickness of 152mm, 178mm, and 203mm. Similarly, a further increase of concrete compressive strength by 25% from 25MPa to 30MPa increased the peak load by 10%, 9.3%, and 9%, respectively, for PVC encased RC walls with core thickness of 152mm, 178mm, and 203mm. Figure 6.4 presents the change in peak load with variation in concrete compressive strength.

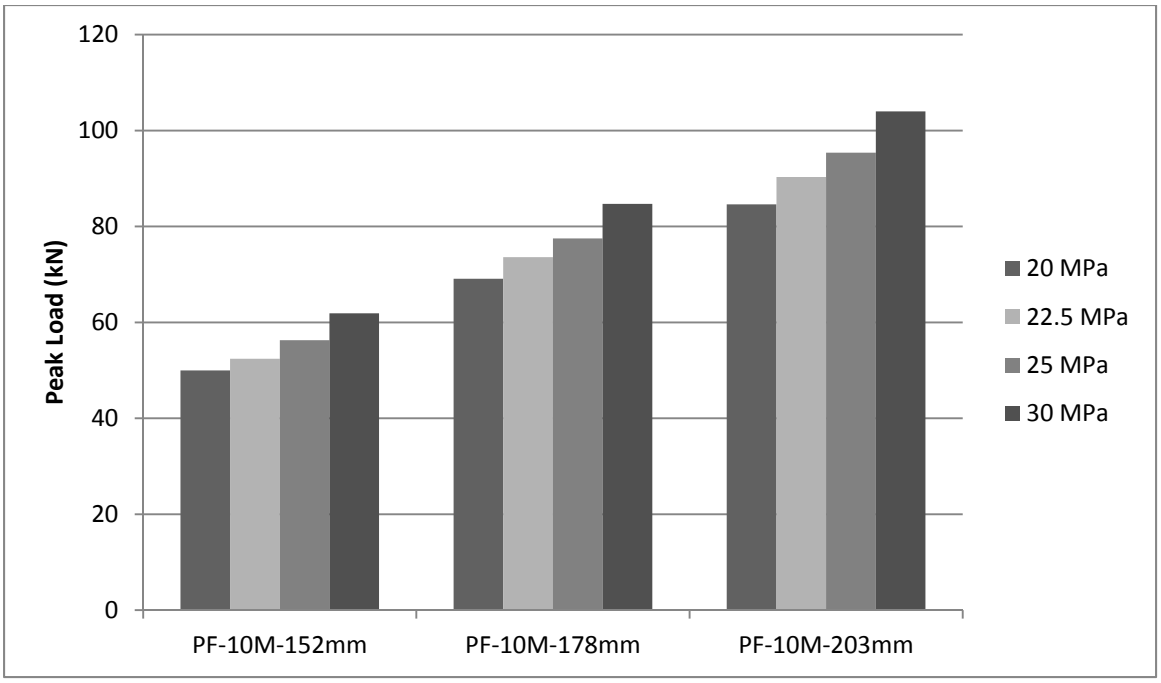

Figure 6.4: Change in Peak Load with Variation in Concrete Compressive Strength for PVC Encased RC Walls

6.2.3 Comparison of RC Walls with and without PVC SIP Formwork

Figure 6.5-6.7 shows the increase in strength versus concrete strength responses of the RC walls with and without PVC encasement. The vertical axis represents the Increase in Strength (%) and the horizontal axis represents the Concrete Compressive Strength (MPa). It can be seen that, as the f_c' increased, the load capacity of the wall also increased. Referring to Figure 6.5, the increase in loading capacity with the increase of f_c' was most significant especially on the PVC encased RC walls. The yield load and peak load improvement was highest between 20 MPa-25 MPa concrete compressive strength. According to Figure 6.6 and Figure 6.7, there is a decrease in improvement with the increase of wall core thickness. This may be due to the reduction in the reinforcement ratio.

According to the results, it is clear that the concrete compressive strength was more effective for RC walls encased with PVC formwork. The average improvement (from simple RC wall to RC wall encased with PVC formwork) for 152mm thick wall was 41%, 38.5%, and 35.5%, respectively, for the

concrete compressive strength of 20MPa, 25MPa, and 30MPa, while the average improvement for 178 mm thick wall was 35.5%, 33%, and 32.5% for the concrete compressive strength of 20MPa, 25MPa, and 30MPa, respectively. For the wall with 203 mm thickness, the average improvement was 29.5%, 16%, and 16%, respectively, for the concrete compressive strength of 20MPa, 25MPa, and 30MPa.

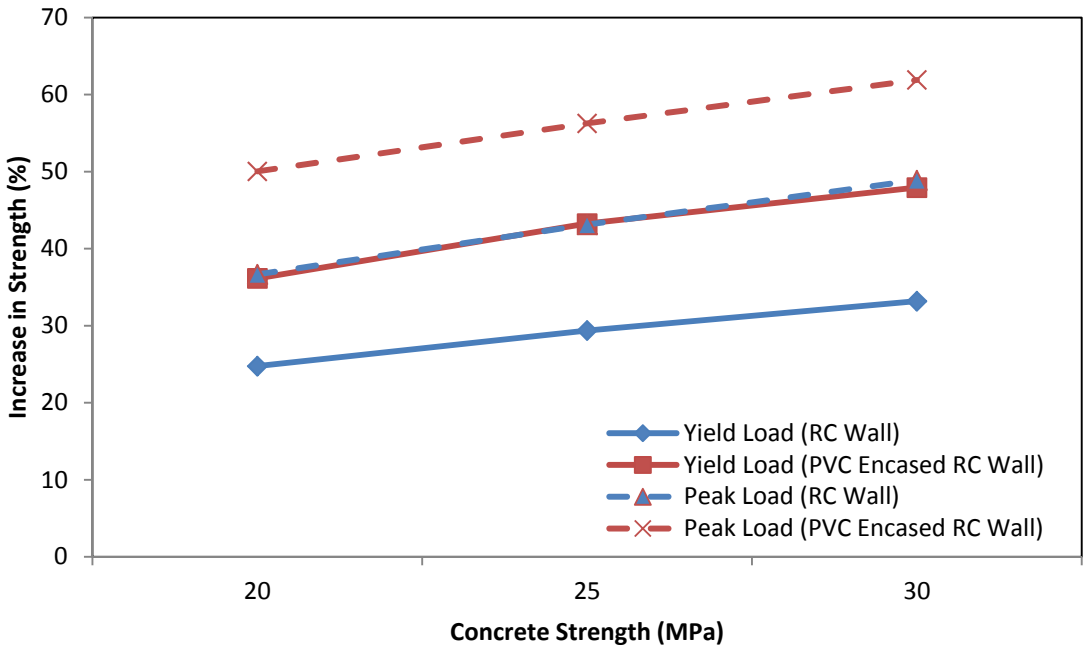

Figure 6.5: Increase in Strength (%) vs Concrete Strength (MPa) for 152mm Thick Walls

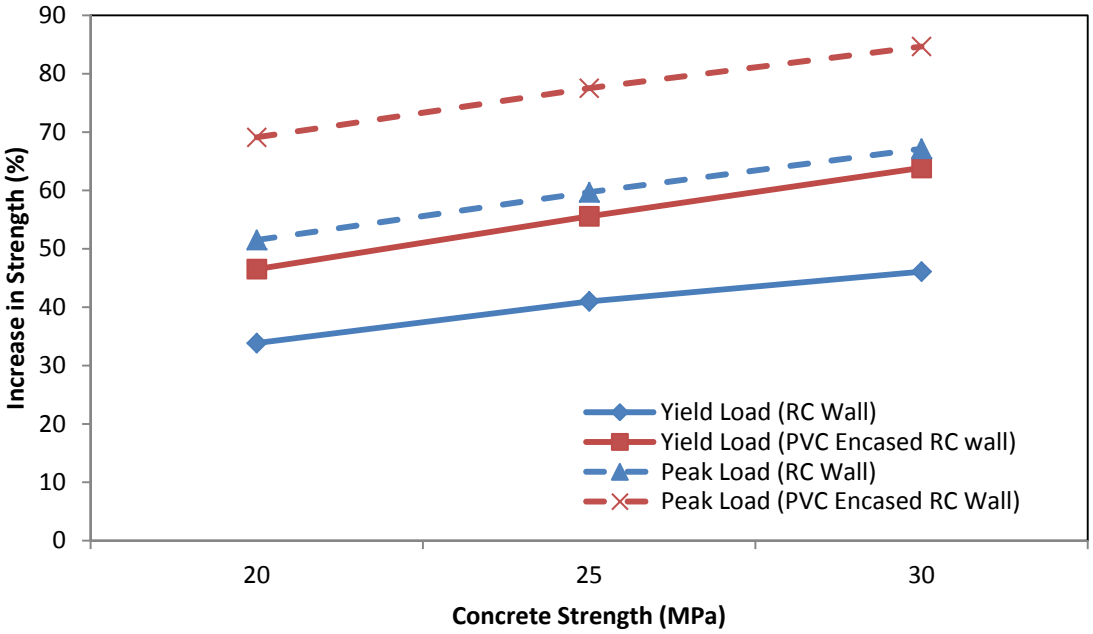

Figure 6.6: Increase in Strength (%) vs Concrete Strength (MPa) for 178mm Thick Walls

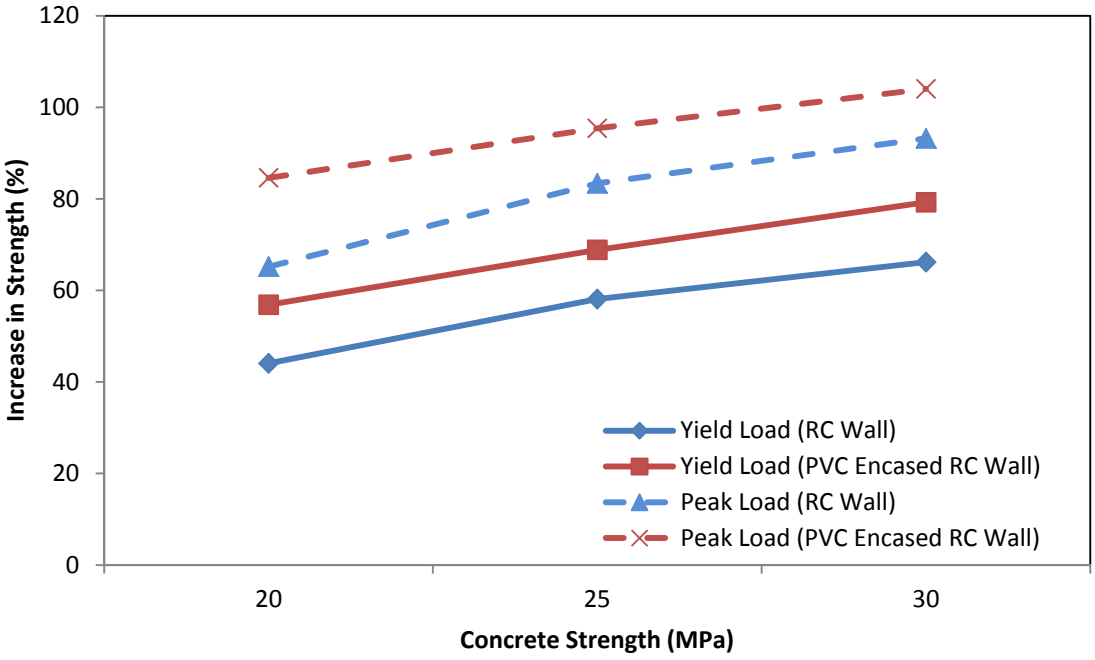

Figure 6.7: Increase in Strength (%) vs Concrete Strength (MPa) for 203 mm Thick Walls

A summary of the improvement in strength between RC walls without PVC encasement and RC walls with PVC encasement with the variation in concrete compressive strength (f_c') is given in Table 6-1. In general, the PVC SIP formwork significantly increased the load carrying capacity of the RC walls. The increase in yield load ranged between 18% and 47% over the RC walls without PVC encasement and the increase in peak load ranged between 12% and 36% over the RC walls without PVC encasement.

Table 6-1: Increase in Strength with Variation in Concrete Compressive Strength for RC Walls with and without PVC Encasement

Wall Thickness (mm)	f_c'	RC Walls without PVC Encasement		RC Walls with PVC Encasement of Flat Panels		Increase in Strength (%)	
-	-	P_{yield} (kN)	P_{peak} (kN)	P_{yield} (kN)	P_{peak} (kN)	P_{yield}	P_{peak}
152	20 MPa	24.75	36.66	36.15	50.03	46%	36%
	25 MPa	29.38	43.11	43.26	56.26	47%	30%
	30 MPa	33.19	48.89	47.93	61.90	44%	27%
178	20 MPa	33.85	51.32	46.53	69.11	37%	34%
	25 MPa	43.8	59.70	55.68	77.52	36%	30%
	30 MPa	46.09	67.15	63.87	84.67	39%	26%
203	20 MPa	44.06	65.19	56.86	84.59	29%	30%
	25 MPa	58.11	83.38	68.85	95.40	18%	14%
	30 MPa	66.18	93.21	79.25	104.02	20%	12%

6.3 Effect of PVC Formwork Thickness

A summary of the load capacity of RC walls with PVC encasement with the variation in PVC formwork thickness is given in Table 6-2. Decreasing the thickness of PVC formwork to half of the original thickness (from 3mm to 1.5 mm) decreased the yield and peak loads by 2.4% and 9.2%, respectively. On the other hand, doubling the thickness (from 3mm to 6 mm) of the PVC formwork increased the load capacity by 2.3% in yield load and by 16% in peak load. Overall, the effect of the PVC formwork thickness was more significant on the peak load than the yield load. Increasing the thickness of the PVC provided additional tensile force reinforcement, hence a higher yield load was reached. Similarly, decreasing the thickness of the PVC reduced the tensile force reinforcement and resulted in a

lower yield load. Figure 6.8 also shows the effect of PVC formwork thickness on the PVC encased RC wall.

Table 6-2: Effect of PVC Formwork Thickness (PF-10M-178mm)

-	RC Wall with PVC Encasement of Flat Panels (t=3mm)		RC Wall with PVC Encasement of Flat Panels (t=1.5mm)		Decrease in Strength (%)		RC Wall with PVC Encasement of Flat Panels (t=6mm)		Increase in Strength (%)	
f_c' MPa	P_{yield} (kN)	P_{peak} (kN)	P_{yield} (kN)	P_{peak} (kN)	P_{yield}	P_{peak}	P_{yield} (kN)	P_{peak} (kN)	P_{yield}	P_{peak}
22.5	49.02	73.58	47.88	67.39	2.4%	9.2%	50.13	85.61	2.3%	16%

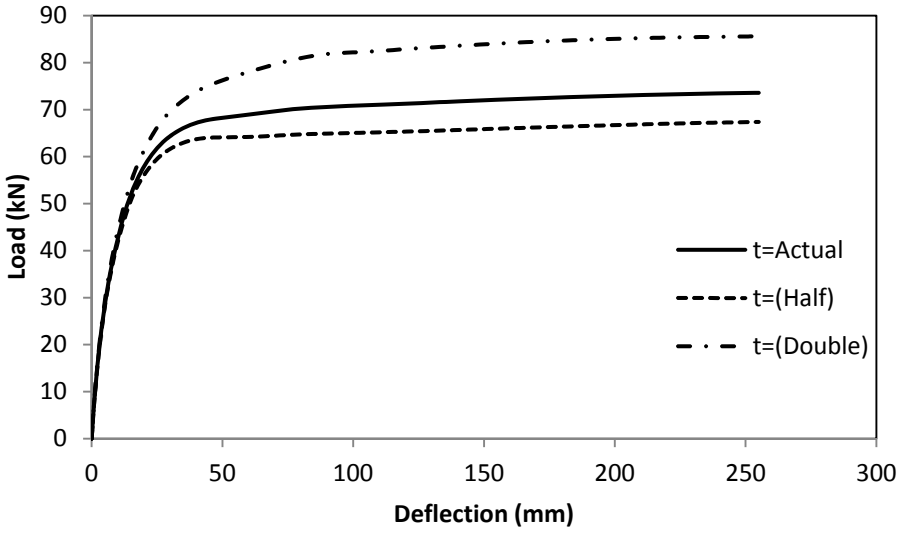

Figure 6.8: Effect of PVC Formwork Thickness (PF-10M-178mm)

6.4 Effect of PVC Strength

Table 6-3 shows the effect of PVC strength on PVC encased RC walls, showing the improvement and decline in load capacity with the variation in PVC tensile strength. Decreasing the PVC strength decreased the yield and peak loads by 1% and 5.2%, respectively. On the other hand, increasing the PVC strength increased the load capacity by 1% in yield load and 5% in the peak load. Again, the effect of the PVC strength was more significant on the peak load as compared to the yield load. Figure 6.9 also shows the effect of PVC strength on the PVC encased RC wall.

Table 6-3: Effect of PVC Strength (PF-10M-178mm)

-	Actual PVC Strength		30% decrease in PVC Strength		Decrease in Strength (%)		30% increase in PVC Strength		Increase in Strength (%)	
f_c' MPa	P_{yield} (kN)	P_{peak} (kN)	P_{yield} (kN)	P_{peak} (kN)	P_{yield} (kN)	P_{peak} (kN)	P_{yield} (kN)	P_{peak} (kN)	P_{yield} (kN)	P_{peak} (kN)
22.5	49.02	73.58	48.56	69.91	1%	5.2%	49.48	77.26	1%	5%

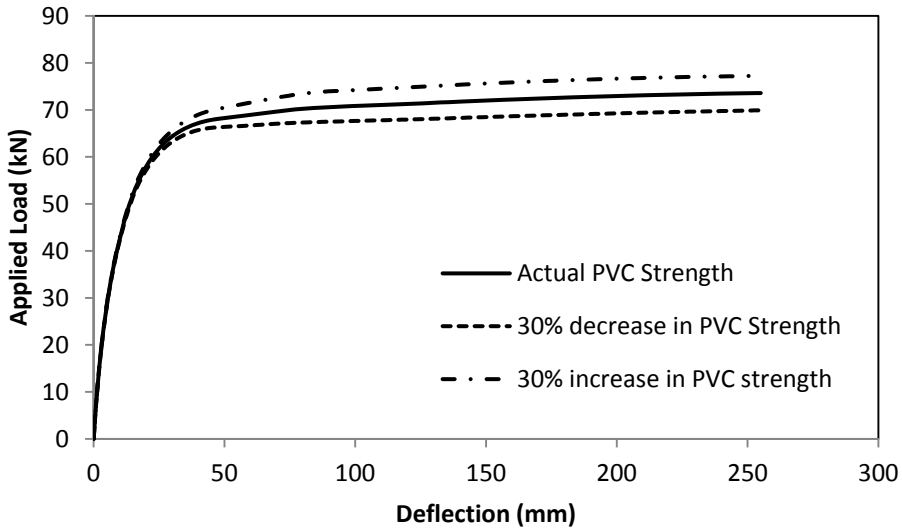

Figure 6.9: Effect of PVC Strength (PF-10M-178mm)

6.5 Summary

The Parametric study provided an in-depth understanding of PVC encasement on RC walls. The concrete compressive strength improved the strength of the RC walls with and without PVC encasement. The maximum increase in strength was observed for RC walls with 20MPa concrete and the lowest increase was observed at 30MPa. This indicates that an increase in concrete strength has a significant effect on the enhancement of yield and peak loads due to encasement of PVC. The effect of PVC formwork thickness and PVC tensile strength were not comparable to the concrete compressive strength. However, increasing the PVC formwork thickness and strength will reduce the reinforcement required for the construction.

Chapter 7: Conclusion and Recommendations

7.1 Summary

The use of PVC SIP formwork has become an increasingly popular tool for concrete structures, providing advantages in labor reduction and construction time. It also provides an enhancement to reinforced concrete strength and ductility. A literature review was performed to determine how PVC SIP formwork affects the behaviour of reinforced concrete. Reinforced concrete encased in SIP formwork tests were also evaluated to identify the area of interest.

The objectives of this thesis were to create and calibrate a RC model for PVC encased RC walls using FE analysis, and then to apply this modelling method to determine the effect of PVC SIP formwork on RC walls. Chapter 3 shows the different modelling techniques investigated to model RC by using a commercial FE software called ABAQUS. The concrete damage plasticity approach was selected. The input commands and the values for this modelling technique were investigated to determine the values which needed to be utilize. These commands and associated inputs are also described in Chapter 3.

Once the modelling approach was determined, FE analyses of reinforced concrete walls with and without PVC SIP formwork were performed based on the actual walls tested in literature (Scott, 2014). 42 3-D nonlinear FE models were developed to simulate the response of RC walls with and without the encasement of PVC SIP formworks. 9 FE models were validated using the experimentally measured data. In addition, the parametric study on concrete compressive strength (f_c'), thickness of PVC SIP formwork and strength of PVC used in formwork was conducted. The results presented included the load carrying capacity and deflection. The suggested modelling procedure has been shown to efficiently and accurately capture the load capacity and load versus deflection behaviour through comparisons between FEM and experimental test results for PVC encased RC walls. The proposed FE models can be used by engineers for the further study and design of PVC encased RC walls.

7.2 Conclusion

Based on the results and discussions presented in the previous chapters, the following conclusions can be drawn.

- The CDP model in the FE software ABAQUS was an appropriate model for the analysis of RC walls encased in PVC SIP formwork.
- Load application as imposed vertical displacement was found to be an appropriate method for evaluating the flexural response of RC walls encased in PVC SIP formwork.
- Results indicate that load versus displacement behaviour from different FEMs is well matched with the experimental results. This thesis verifies the accuracy of the proposed material model using experimental results for RC elements subjected to flexural loading.
- The solid elements (C3D8R) were the preferred method for the modelling of concrete and longitudinal reinforcing bars. The reinforcement steel strain values as calculated by FE model were also in good agreement with the experimental results.
- The shell elements (S4R) were the preferred method of modelling the PVC SIP formwork.
- The perfect bond between components of the FE model was the preferred method of modelling RC walls encased in PVC SIP formwork.
- The parametric study performed showed that the change in PVC SIP formwork thickness or the strength of PVC had the most effect on the peak load of walls (without PVC encasement or with PVC encasement). The change in concrete compressive strength had the maximum effect between 20 MPa and 25 MPa.

7.3 Recommendations

The current research work has developed a better understanding of the FE modelling of the structural behaviour of RC encased in PVC formwork. It has also contributed to the understanding of the

material modelling and effect of concrete compressive strength on the yield and ultimate loads for these structures. However, some further investigation and validation are recommended:

- A realistic description of bond action between concrete and steel is one of the crucial steps. A proper pull-out test before modelling any kind of RC structure is required.
- Future experimental work for PVC encased RC walls can be designed using the proposed FEA based methodology.
- Moreover, as computer and software facilities become more powerful, both concrete and reinforcement can be simulated in greater details to provide a better prediction.
- The developed FEA based methodology can be used to investigate the reinforcement ratio using FRP SIP formwork.
- Damage parameters for concrete in compression and tension need to be investigated further.

Bibliography

ABAQUS (2011). "*Theory Manual, and User Manual Version 6.11*". Dassault Systems Simulia Corp, Providence, RI.

ACI 440.R1-06., (2006). "*Guide for the Design and Construction of Structural Concrete Reinforced with FRP Bar*s". ACI 440.IR-06.

Amr, A. H., (2014). "*Behaviour of PVC Encased Reinforced Concrete Walls under Axial Eccentric Loading*". MASc Thesis, University of Waterloo, Waterloo, Ontario, Canada.

Avila, M. L., Quevedo, R. L., & Morfa, C. R., (2009). "*Evaluating Longitudinal Shear Resistance in Composite Slabs with Steel Decks*". RevistaIngenieria de Construccion, Vol (24):95-113.

Benjamin, S., (2014). "*Flexural Behaviour of Stay-in-place PVC Encased Reinforced Concrete Walls with Various Penal Types*". MASc Thesis, University of Waterloo, Waterloo, Ontario, Canada.

Belarbi, A., & Hsu, T., (1994). "*Constitutive Laws of Concrete in Tension and Reinforcing Bars Stiffened by Concrete*". ACI Structural Journal, 91(4):465-474.

Chahrour, A. H., Soudki, K. A., & Staube, J. (2005). "*RBS Polymer Encased Wall part I: Experimental and Theoretical Provisions for Flexural and Shear*". Construction and Building Materials, 550-563.

Collins, M. P., & Mitchell, D., (1987). "*Prestressed Concrete Structures*". Toronto: Response publications.

Dieter, D. A., & Dietsche, J. S. (2006). "*Construction Bridge Decks Constructed with Fiber-Reinforced Stay-in-place Forms and Grid Reinforced*". Transportation Research Record, 219-226.

Fam, A., & Nelson, M. (2014). "*Full Bridge Testing at Scale Construction with Novel FRP Stay-in-place Structural forms for Concrete Deck*". Construction and Bridge Materials, 368-376.

Fam, A. Z., & Rizkalla, S. H. (2002). "*Flexural Behaviour of Concrete-Filled Fiber-Reinforced Polymer Circular Tubes*". Journal of Composites for Construction, 123-132.

Gai, X., & Darby, A. (2014). "*Experimental Investigation into a Ductile FRP Stay-in-place Formwork System for Concrete Slabs*". Construction and Building Materials, 1013-1023.

Garg, A. K., & Abolmaali, A. (2009). "*Finite-Element Modelling and Analysis of Reinforced Concrete Box Culverts*". Journals of Transportation Engineering, Vol (135):121-128.

Hsu, T., & Zhang, L. (1996). "Tension *Stiffening in Reinforced Concrete Member Elements*". ACI Structural Journal, 93(1):108-115.

Kmiecik, P., & Kaminski, M. (2011). "Modelling *of Reinforced Concrete Structures and Composite Structures with Concrete Strength Degradation taken into Consideration*". Archives of Civil and Mechanical Engineering, 11(3):623-636.

Kuder, K. G., Gupta, R., Harris-Jones, C., Hawksworth, R., Hendersong, S., & Whitney, J. (2009). "*Effect of PVC Stay-in-place Formwork on Mechanical Performance of Concrete*". Journal of Materials in Civil Engineering, 307-315.

Lee, J., & Fenves, G. L. (1998). "*Plastic-Damage Model for Cyclic Loading of Concrete*." Journal of Engineering Mechanics, 124(8):892-900.

Lubliner, J., Oliver, J., Oller, S., & Onate, E. (1989)."*A Plastic-Damage Model for Concrete*". International Journal Solids Structures, 25(3):229-326.

McClelland, R., (2007) "*Permanent formwork for Composite Bridge Deck*". Concrete, 10-11.

Mohamed, H. M., & Masmoudi, R. (2012). "*Effect of Test Parameters on Flexural Strength of Circular Fiber-Reinforced Concrete Beams*". Journal of Reinforced Plastics and Composites, 897-914.

Muniruzzaman, P. K. (2013). "*Numerical Investigation of the Effectiveness of FRP and TRM in Repairing Corrosion Damaged Reinforced Concrete Beams*". Master's Thesis, University of British Columbia, Okanagan, Canada.

Obaidat, Y. (2011). "*Structural Retrofitting of Concrete Beams using FRP-Deboning Issues*". PhD Thesis, Lund University, Lund, Sweden.

Octaform General Guide: Version 2, Revision 1. Vancouver (BC): Octaform System Inc; 2004. 87p.

Ren, W., Sneed, L., Yang, Y., & He R. (2014). "*Numerical Simulation of Prestressed Precast Concrete Bridge Deck Panels Using Damage Plasticity Model*". International Journal of Concrete Structures and Materials, 2234-1315.

Rteil, A. A., Soudki, K. A., & Richardson, D. J. (2008). "*Flexural Behaviour of Octaform Forming System*". ACI Special Publication, 133-148.

Tamai, S. (1988). "Average Stress-Strain Relationship in Post Yield Range of Steel Bar in Concrete". Concrete Library, JSCE (11):117-129.

Tahmasebinia, F. (2008). *"Finite Element Simulation of Reinforced Concrete Structure under Impact Accident*." Structure Survey, Vol(26):445-454

Tuo, L. (2008). "*Application of Damaged Plasticity Model for Concrete*". Structural Engineers, 24(2):22-27.

Wahab, N., & Soudki, K, A. (2013). "*Flexural Behaviour of PVC Stay-in-place Formed Walls*". Journal of Construction and Building Materials, 830-839.

Wang, T., & Hsu, T. (2001). "*Nonlinear Finite Element Analysis of Concrete Structures using New Constitutive Models*". Computers and Structures, 79(32):2791-2791.